Article

Asymmetric tris-Heteroleptic IridiumIII Complexes Containing 9-phenyl-9-phosphafluorene Oxide Moiety with Enhanced Charge Carrier Injection/Transporting Properties for Highly Efficient Solution-Processed Organic Light-Emitting Diodes (OLEDs)

Xianbin Xu, Haoran Guo, Jiang Zhao, Boao Liu, Xiaolong Yang, Guijiang Zhou, and Zhaoxin Wu

Chem. Mater., **Just Accepted Manuscript** • DOI: 10.1021/acs.chemmater.6b03177 • Publication Date (Web): 08 Nov 2016

Asymmetric *tris*-Heteroleptic Iridium^{III} Complexes Containing 9-phenyl-9-phosphafluorene Oxide Moiety with Enhanced Charge Carrier Injection/Transporting Properties for Highly Efficient Solution-Processed Organic Light-Emitting Diodes (OLEDs)

Xianbin Xu,[†] Haoran Guo,[†] Jiang Zhao,[†] Boao Liu,[†] Xiaolong Yang,[†] Guijiang Zhou,*[,†] and Zhaoxin Wu*[,‡]

[†]MOE Key Laboratory for Nonequilibrium Synthesis and Modulation of Condensed Matter, Department of Chemistry, School of Science, State Key Laboratory for Mechanical Behavior of Materials, Xi'an Jiaotong University, Xi'an 710049, People's Republic of China

[‡]Key Laboratory of Photonics Technology for Information, School of Electronic and Information Engineering, Xi'an Jiaotong University, Xi'an, 710049, People's Republic of China

ABSTRACT

Cyclometalating ligand containing 9-phenyl-9-phosphafluorene oxide (PhFlPO) moiety has been synthesized and used to construct asymmetric *tris*-heteroleptic cyclometalating Ir^{III} complexes in combination with other ppy-type (Hppy = 2-phenylpyridine) ligands containing functional group with different charge carrier injection/transporting character. Their photophysical properties, electrochemical behaviors and electroluminescent (EL) performances have been characterized in detail. Time-dependent density functional theory (TD-DFT) and natural transition orbital (NTO) calculation was carried out to gain insight into the photophysical properties of these complexes. The NTO results show that the characters of the lowest triplet excited states (T_1) can be delicately manipulated through the combination of different cyclometalating ligands. In addition, the strong electron injection/transporting (EI/ET) ability associated with the PhFlPO moiety can confer EI/ET properties to the asymmetric *tris*-heteroleptic cyclometalating Ir^{III} complexes. Consequently, the solution-processed organic light-emitting diodes/devices (OLEDs) based on these asymmetric *tris*-heteroleptic Ir^{III} phosphorescent complexes can exhibit outstanding electroluminescent (EL) performances with the maximum external quantum efficiency (η_{ext}) of 19.3%, current efficiency (η_L) of 82.5 cd A^{-1} and power efficiency (η_P) of 57.3 lm W^{-1} for the yellow-emitting device. These results show the great potential of PhFlPO moiety in developing phosphorescent emitters and functional materials with excellent EI/ET properties.

INTRODUCTION

Stimulated by the discovery of phosphorescent (triplet) emitters, especially the ppy-type (Hppy=2-phenylpyridine) cyclometalated Ir^{III} complexes,[1-2] the organic light-emitting diodes/devices (OLEDs) pertinent technologies, both materials[3-5] and device architectures,[6] have gone through rapid development during the past two decades. Typically, the phosphorescent emitters are dispersed into an appropriate host material to alleviate the detrimental triplet-triplet annihilation (TTA) and undesired aggregation/excimer formation.[7] According to OLEDs operating mechanism, charge carrier injection/transporting and balance are vital to the electroluminance (EL) performance of phosphorescent OLEDs (PHOLEDs) and their longevity.[8] Therefore, functional materials with hole injection/transporting (HI/HT) and/or electron injection/transporting (EI/ET) character are usually employed to construct multilayered OLEDs in order to both reduce charge carrier injection barrier and to achieve balanced charge carrier injection/transporting.[6] In addition, bipolar hosts incorporating functional groups with both HI/HT and EI/ET features have also gained substantial research endeavors due to their capability of balancing both kinds of charge carrier transporting and broadening the recombination zone.[9-10] Moreover, functionalization of the cyclometalated Ir^{III} complexes through introducing functional groups with HI/HT and/or EI/ET traits to their ligands represents another crucial strategy to improve the EL performances of the concerned OLEDs.[8] Unfortunately, organic semiconductors typically favor hole transporting process with the mobility of two to three orders of magnitude higher than that for electron.[11] Therefore, developing materials with superior EI/ET properties is more urgent in view of achieving balanced charge carrier injection/transporting in OLEDs to enhance EL efficiencies.

So far, however, only a few functional groups, including oxadiazole,[12-14] diarylsulfone,[15-20] imidazole [21-22], organoboron[23-24] and aryl phosphine oxide (APO)[25] moieties, have been proven to be capable of conferring decent EI/ET character to the Ir^{III} triplet emitters through ligand substitution. Among them, APO moieties represent the most investigated EI/ET functional groups. Taking advantage of their intrinsic electronic properties, APO moieties have been widely used as building blocks to construct both electron injection/transporting materials and bipolar hosts with superior EI/ET features.[25] Nevertheless, as the one of the determinants of the EL performance of OLEDs, cyclometalated Ir^{III} complexes incorporating APO moieties are still very rare to date. Zhou and co-workers have demonstrated that introducing of diphenylphosphine oxide ($POPh_2$) moiety into the phenyl rings of the traditional green-emitting $(ppy)_2Ir(acac)$ and *fac*-$Ir(ppy)_3$ can indeed confer EI/ET characters to Ir^{III} triplet emitters.[16, 19] A serial of functionalized Ir^{III} triplet emitters with the $POPh_2$ moieties have also been developed by Li and co-workers to show attractive EL performances.[26] In 2012, Fan and co-workers reported the solution-processed blue PHOLEDs using $POPh_2$-functionalized bis(2-(4',6'-difluoro)phenylpyridinatoN,$C^{2'}$)$_2$iridium(III) picolinate (FIrpic) as the triplet dopant.[27] Also, phosphorescent dendrimers with $POPh_2$ moieties have also been prepared to make high-performance solution-processed PHOLEDs owing to the enhanced EI/ET properties.[28-29] Clearly, all these encouraging results have indicated the great potential and feasibility of APO moieties of affording organic semiconductors with excellent EI/ET features.

During the past decade, phosphafluorene (or phosphole) was discovered to be an excellent EI/ET moiety and has also gained substantial amount of research efforts as building block to construct π-conjugated materials with attractive EI/ET features for various applications

including OLEDs.[30-35] However, to our knowledge, no phosphorescent emitters incorporating phosphafluorene (or phosphole) moiety has been reported. On account of the only handful of APO-functionalized Ir^{III} triplet emitters and the excellent EI/ET properties of phosphafluorene moiety, it is rational to further exploit the potential of phosphafluorene moiety in constructing Ir^{III} triplet emitters with superior EI/ET and/or bipolar properties. Herein, we present a serial of asymmetric *tris*-heteroleptic cyclometalated Ir^{III} complexes incorporating ppy-type ligands bearing 9-phenyl-9-phosphafluorene oxide (PhFlPO) moiety (**L-PO**, **Scheme 1**). Based on our previously results[16-18, 24], diphenylamine (NPh_2) moiety is an excellent HI/HT functional group whereas $B(Mes)_2$ possesses unique electronic properties both in modulating the emission spectra of the concerned Ir^{III} complexes and endowing the resulting Ir^{III} complexes with EI/ET abilities. Besides, Ir^{III} complexes incorporating phenoxy (OPh) moiety normally show a good balance between HI/HT and EI/ET and devices based on these complexes deliver excellent performance. With the intention to develop Ir^{III} complexes with superior EI/ET and/or ambipolar character and delicately manipulate the charge carrier injection/transport properties of Ir^{III} complexes, ppy-type ligands incorporating these functional groups, *i.e.* **L-N**, **L-O** and **L-B** (**Scheme 1**), were chosen to construct asymmetric *tris*-heteroleptic Ir^{III} complexes along with ligand **L-PO**. The significantly lowered LUMO levels and substantially higher electron-only current density of these complexes than that of the famous host material CBP justified the effectiveness of incorporating PhFlPO for facilitating EI/ET. The solution-processed OLEDs based on these emitters can show excellent EL performance with the maximum efficiencies of 82.5 cd A^{-1}, 57.3 lm W^{-1} and EQE of 19.3%. All these results not only demonstrate the great potential of the PhFlPO moiety in furnishing excellent EI/ET capacity, but also provide an alternative approach to design phosphorescent emitters with superior EI/ET and/or bipolar features.

EXPERIMENTAL SECTION

General information. Commercially available reagents were used without further purification unless otherwise stated. All reactions were conducted under a nitrogen atmosphere and no special precautions were required during the workup. Solvents were carefully dried and distilled from appropriate drying agents prior to use. All reactions were monitored by thin-layer chromatography (TLC) from Merck & Co., Inc. Flash column chromatography and preparative TLC was carried out using silica gel from Shenghai Qingdao (200–300 mesh). ^{1}H, ^{13}C, and ^{31}P NMR spectra were recorded in $CDCl_3$ on a Bruker Avance 400 MHz spectrometer and the chemical shifts were referenced to the solvent residual peak at δ 7.26 ppm for ^{1}H and 77.0 ppm for ^{13}C, respectively. Fast atom bombardment mass spectrometry (FAB-MS) spectra were recorded on a Finnigan MAT SSQ710 system. UV/Vis spectra were recorded on a Shimadzu UV-2250 spectrophotometer. The photoluminescent spectra and lifetimes of the asymmetric Ir^{III} complexes were recorded on an Edinburgh Instruments FLS920 spectrophotometer. The phosphorescence quantum yields (Φ_P) were determined in CH_2Cl_2 solutions at 293 K against *fac*-[$Ir(ppy)_3$] standard (Φ_P *ca.* 0.40). The absolute Φ_P of CBP films doped with these Ir^{III} complexes were measured in an integrating sphere. Cyclic voltammetry measurements were carried out on a Princeton Applied Research model 2273A potentiostat at a scan rate of 100 mV s^{-1}. A conventional three-electrode configuration with a glassy carbon working electrode, a Pt-sheet counter electrode, and a Pt-wire reference electrode was used. The supporting electrolyte was 0.1 M $[Bu_4N]PF_6$ in tetrahydrofuran (THF). Ferrocene was added as a calibrant after each set of measurements, and all potentials reported are quoted with reference to the ferrocene/ferrocenium (Fc/Fc^{+}) couple.

Synthesis. The organic ppy-type ligands **L-N**, **L-O** and **L-B** have been prepared successfully according to the literature method.[16]

2-(4-Bromophenyl)pyridine (1): Under a nitrogen atmosphere, 4.74 g (30 mmol) 2-bromopyridine, 6.32 g (31.5 mmol) (4-bromophenyl)boronic acid, 1.73 g (1.5 mmol) $Pd(PPh_3)_4$, 40 mL THF and 20 mL potassium carbonate (K_2CO_3, 2M） were added into a SCHLENk flask and then the flask was sealed. The reaction mixture was heated to 110 °C and stirred for 16 h. After cooling to room temperature, the reaction mixture was extracted with dichloromethane (CH_2Cl_2) and dried over anhydrous sodium sulfate (Na_2SO_4). The extracts were combined and concentrated. The crude product was purified on column chromatography on silica gel (CH_2Cl_2:PE=1:1, v/v, PE=petroleum ether) to give the target product as a white solid (5.96 g; Yield: 85.0%). ^{1}H NMR (400 MHz, $CDCl_3$): δ (ppm) 8.68 (d, J = 4.8 Hz, 1 H), 7.87 (d, J = 8.0 Hz, 2 H), 7.75 (t, J = 7.2 Hz, 1 H), 7.70 (t, J = 8.0 Hz, 1 H), 7.60 (d, J = 8.4 Hz, 2 H), 7.26-7.23 (m, 1 H); ^{13}C NMR (100 MHz, $CDCl_3$): δ (ppm) 156.23, 149.76, 138.23, 136.87, 131.86, 128.44, 123.42, 122.41, 120.28; FAB-MS (m/z): 233, 235 $[M]^+$; Anal. Calcd. for $C_{11}H_8BrN$: C, 56.44; H, 3.44; N, 5.98; found: C, 56. 29; H, 3.31; N, 5.87%.

(4-(Pyridin-2-yl)phenyl)boronic acid (2): Under a nitrogen atmosphere, 11.2 mL *n*-butyllithium (2.5 M in hexane) was added dropwise with syringe into a solution of 5.0 g (21.36 mmol) compound **1** in 30 mL THF (dry) at -78 °C and stirred for 1 hour. Then, 7.4 mL (64.08 mmol) trimethyl borate ($B(OMe)_3$) was added into the reaction mixture with syringe and the reaction mixture was allowed to warm to room temperature and stirred for another 16 h. Water was added, and the reaction mixture was extracted with CH_2Cl_2 and dried over anhydrous Na_2SO_4. After the solution was concentrated, petroleum ether was added and white precipitate was formed. The white precipitate was collected by filtration and dried in vacuum to give the

product as a white solid (2.80 g; Yield: 65.8%). ^{1}H NMR (400 MHz, acetone-d_6): δ (ppm) 7.72 (d, J = 4.4 Hz, 1 H), 7.15 (d, J = 8.4 Hz, 2 H), 7.04-6.99 (m, 3 H), 6.94-6.90 (m, 1 H), 6.45 (s, 2 H), 6.38 (t, J = 5.6 Hz, 1 H); FAB-MS (m/z): 199 [M] $^+$; Anal. Calcd. for $C_{11}H_{10}BNO_2$: C, 66.39; H, 5.06; N, 7.04; found: C, 66.18; H, 5.23; N, 6.87%.

2-(2'-Bromo-[1,1'-biphenyl]-4-yl)pyridine (3): Under a nitrogen atmosphere, 2.80 g (14.0 mmol) compound **2**, 3.32 g (14.0 mmol) 1,2-dibromobenzene, 0.81 g (0.70 mmol) $Pd(PPh_3)_4$, 30 mL THF and 15 mL K_2CO_3 (2M) were addd into a SCHLENK flask and then the flask was sealed. The reaction mixture was heated to 110 °C and stirred for 16 h. After cooling to room temperature, the reaction mixture was extracted with CH_2Cl_2 and dried over anhydrous Na_2SO_4. The extracts were combined and concentrated. The cude product was purifed on column chromatography on silica gel (PE:Et_2O=5:1, v/v, Et_2O=diethyl ether) to give the target product as a white solid (3.12g; Yield: 71.5%). ^{1}H NMR (400 MHz, $CDCl_3$): δ (ppm) 8.72 (d, J = 4.4 Hz, 1 H), 8.08 (d, J = 7.6 Hz, 2 H), 7.80-7.74 (m, 2 H), 7.69 (d, J = 7.6 Hz, 1 H), 7.55 (d, J = 7.6 Hz, 2 H), 7.37 (d, J = 4.4Hz, 2 H), 7.26-7.20 (m, 2 H); ^{13}C NMR (100 MHz, $CDCl_3$): δ (ppm) 156.93, 149.67, 142.02, 141.59, 138.53, 136.71, 133.13, 131.18, 129.79, 128.81, 127.37, 126.46, 122.47, 122.15, 120.49; FAB-MS (m/z): 309, 311 [M] $^+$; Anal. Calcd. for $C_{17}H_{12}BrN$: C, 65.83; H, 3.90; N, 4.52; found: C, 65.71; H, 3.79; N, 4.45%.

Phenyl(4'-(pyridin-2-yl)-[1,1'-biphenyl]-2-yl)phosphine oxide (4): Under a nitrogen atmosphere, 0.21 g (8.86 mmol) magnesium turnings was placed in a three-necked bottle and 15 mL anhydrous THF was added into the bottle with syringe. A bead of iodine was added. A solution of 2.5 g (8.06 mmol) compound **3** in 15 mL anhydrous THF was added dropwise into the above mixture with dropping funnel over 10 min. Then, the reaction mixture was heated to 80 °C and stirred for 1 h. After cooling to room temperature, a solution of 2.16 g (12.10 mmol)

dichlorophenylphosphine ($PhPCl_2$) in 10 mL anhydrous THF was added dropwise into the reaction mixture with dropping funnel over 10 min. After that, the reaction mixture was heated to 80 °C and stirred for 16 h. Then, the reaction mixture was cooled to 0 °C and water was added. The reaction mixture was extracted with CH_2Cl_2 and dried over anhydrous Na_2SO_4. The solution was concentrated and the product was isolated on column chromatography on silica gel (ethyl acetate, AcOEt) to give a light yellow liquid oil (1.13 g; Yield: 39.5%). ^{1}H NMR (400 MHz, $CDCl_3$): δ (ppm) 8.71 (d, *J* = 4.4 Hz, 1 H), 8.00-7.93 (m, 3 H), 7.81-7.73 (m, 2 H), 7.62 (t, *J* = 7.6 Hz, 1 H), 7.53 (t, *J* = 7.6 Hz, 1 H), 7.44-7.25 (m, 10 H); ^{13}C NMR (100 MHz, $CDCl_3$): δ (ppm) 156.71, 149.79, 145.40, 139.88, 139.82, 139.01, 136.92, 132.86, 132.76, 132.31, 131.98, 130.70, 130.59, 130.47, 129.88, 129.75, 128.52, 128.39, 127.78, 127.66, 126.74, 122.42, 120.60; ^{31}P NMR (162 MHz, $CDCl_3$): δ (ppm) 18.35; FAB-MS (m/z): 355 $[M]^+$; Anal. Calcd. for $C_{23}H_{18}NOP$: C, 77.74; H, 5.11; N, 3.94; found: C, 77.59; H, 4.88; N, 3.79%.

5-Phenyl-3-(pyridin-2-yl)benzo[b]phosphindole-5-oxide (L-PO) : Under a nitrogen atmosphere, 1.13 g (3.18 mmol) compound **4**, 36 mg (0.16 mmol) $Pd(OAc)_2$ and 20 mL anhydrous THF were added into a SCHLENK flask. The flask was sealed and the reaction mixture was heated to 65 °C and stirred for 16 h. After cooling to room temperature, the reaction mixture was concentrated and the product was isolated on column chromatography on silica gel (AcOEt) to give the product as a white solid (0.94 g; Yield: 86.5%). ^{1}H NMR (400 MHz, $CDCl_3$): δ (ppm) 8.66 (d, *J* = 4.8 Hz, 1 H), 8.31 (t, *J* = 9.6 Hz, 2 H), 7.93 (dd, *J* = 2.8, 8.0 Hz, 1 H), 7.87 (dd, *J* = 2.8, 7.6 Hz, 1 H), 7.74-7.65 (m, 5 H), 7.61 (t, *J* = 8.0 Hz, 1 H), 7.48 (t, *J* = 7.6 Hz, 1 H), 7.42-7.36 (m, 3 H), 7.26-7.22 (m, 1 H); ^{13}C NMR (100 MHz, $CDCl_3$): δ (ppm) 155.74, 149.74, 142.32, 142.10, 141.50, 141.29, 140.62, 140.51, 136.94, 134.00, 133.47, 132.94, 132.76, 132.25, 132.22, 132.16, 132.14, 131.16, 131.05, 129.98, 129.89, 129.69, 129.57, 128.82, 128.70,

128.21, 128.11, 122.68, 121.65, 121.55, 121.52, 121.42, 120.49; ^{31}P NMR (162 MHz, $CDCl_3$): δ (ppm) 33.55; FAB-MS (m/z): 353 $[M]^+$; Anal. Calcd. for $C_{23}H_{16}NOP$: C, 78.18; H, 4.56; N, 3.96; found: C, 77.92; H, 4.49; N, 3.89%.

General Procedure for Synthesis of the *tris*-Heteroleptic Ir^{III} Cyclometalated Complexes: Under a nitrogen atmosphere, a solution of 1.0 equivalent of **L-PO**, **L-N/L-O/L-B** and $IrCl_3 \cdot nH_2O$ each in a mixture of THF and water (3:1, v/v) were heated to 110 °C and stirred for 16 h in a sealed SCHLENK flask. After cooling to room temperature, the reaction mixture was extracted with CH_2Cl_2 and the dried over anhydrous Na_2SO_4. After concentrated, petroleum ether was added into the solution and the cyclometalated Ir^{III} μ-chloro-bridged dimer was formed as colored precipitates, which were collected by filtration and dried in vacuum. Then, the Ir^{III} μ-chloro-bridged dimer and thallium(I) acetylacetonate [Tl(acac)] (2.2 equivalent) were added into anhydrous CH_2Cl_2 and stirred at room temperature for 16 h. The reaction mixture was concentrated and the product was isolated with preparative thin-layer chromatography on silica gel with appropriate eluent. ***Caution!*** *The reactant thallium(I) acetylacetonate [Tl(acac)] is extremely toxic and should be dealed very carefully!*

Ir-PON: CH_2Cl_2:AcOEt=1:1(v/v); Yield: 13.8%. ^{1}H NMR (400 MHz, $CDCl_3$): δ (ppm) 8.47 (d, *J* = 5.6 Hz, 1 H), 8.29 (d, *J* = 4.2 Hz, 1 H), 7.79-7.75 (m, 3 H), 7.70-7.65 (m, 2 H), 7.61 (t, *J* = 8.0 Hz, 1 H), 7.54 (d, *J* = 8.0 Hz, 1 H), 7.45-7.34 (m, 6 H), 7.33-7.22 (m, 3 H), 7.14 (m, 5 H), 6.96-6.91 (m, 7 H), 6.80 (d, *J* = 2.8 Hz, 1 H), 6.48 (dd, *J* = 2.4, 8.4 Hz, 1 H), 5.50 (d, *J* = 2.4 Hz, 1 H), 1.84 (s, 3 H), 1.80 (s, 3 H); ^{13}C NMR (100 MHz, $CDCl_3$): δ (ppm) 184.92, 184.77, 168.22, 166.63, 158.99, 148.18, 148.00, 147.85, 147.08, 147.01, 146.88, 146.42, 142.45, 142.23, 141.23, 141.01, 137.10, 136.94, 136.70, 132.42, 131.70, 131.24, 131.14, 129.42, 129.33, 128.98, 128.90, 128.57, 128.45, 125.93, 125.80, 125.70, 124.62, 124.23, 124.13, 124.03, 123.16, 121.96, 121.42,

121.32, 120.01, 118.90, 117.96, 113.89, 100.64, 28.83, 28.76; ^{31}P NMR (162 MHz, $CDCl_3$): δ (ppm) 33.96; FAB-MS (*m/z*): 988 $[M+Na]^+$; Anal. Calcd. for $C_{51}H_{39}IrN_3O_3P$: C, 63.47; H, 4.07; N, 4.35; found: C, 63.29; H, 3.89; N, 4.28%.

Ir-POO: CH_2Cl_2:AcOEt=1:1(v/v); Yield: 16.5%. ^{1}H NMR (400 MHz, $CDCl_3$): δ (ppm) 8.51 (d, *J* = 5.6 Hz, 1 H), 8.41 (d, *J* = 4.2 Hz, 1 H), 7.84-7.81 (m, 3 H), 7.74-7.59 (m, 5 H), 7.48 (d, *J* = 8.8 Hz, 1 H), 7.44 (dd, *J* = 1.6, 7.6 Hz, 1 H), 7.38-7.34 (m, 3 H), 7.24-7.18 (m, 5 H), 7.09 (t, *J* = 7.2 Hz, 1 H), 7.02 (t, *J* = 7.6 Hz, 1 H), 6.89 (d, *J* = 8.8 Hz, 2H), 6.75 (d, *J* = 3.2 Hz, 1 H), 6.38 (dd, *J* = 2.4, 8.4 Hz, 1 H), 5.66 (d, *J* = 2.4 Hz, 1 H), 5.26 (s, 1 H), 1.84 (s, 3 H), 1.80 (s, 3 H); ^{13}C NMR (100 MHz, $CDCl_3$): δ (ppm) 185.08, 184.71, 168.11, 166.83, 158.56, 158.41, 155.86, 148.30, 148.11, 148.07, 146.93, 146.81, 142.39, 142.17, 141.24, 141.03, 138.91, 137.19, 134.74, 133.69, 132.37, 132.28, 131.72, 131.70, 131.23, 131.12, 129.38, 129.33, 128.98, 128.87, 128.55, 128.42, 125.68, 125.59, 125.35, 124.40, 124.36, 124.25, 123.40, 123.27, 122.04, 121.33, 121.24, 120.75, 120.33, 118.93, 118,32, 110.40, 100.65, 28.77, 28.75; ^{31}P NMR (162 MHz, $CDCl_3$): δ (ppm) 33.89; FAB-MS (*m/z*): 913 $[M+Na]^+$; Anal. Calcd. for $C_{45}H_{34}IrN_2O_4P$: C, 60.73; H, 3.85; N, 3.15; found: C, 60.59; H, 3.93; N, 3.05%.

Ir-POB: CH_2Cl_2:AcOEt=1:1(v/v); Yield: 12.7%. ^{1}H NMR (400 MHz, $CDCl_3$): δ (ppm) 8.62 (d, *J* = 5.6 Hz, 1 H), 8.28 (d, *J* = 5.6 Hz, 1 H), 7.97 (d, *J* = 8.0 Hz, 1 H), 7.86 (t, *J* = 8.0 Hz, 1 H), 7.81 (d, *J* = 10.4 Hz, 1 H), 7.69-7.56 (m, 4 H), 7.49 (d, *J* = 8.0 Hz, 1 H), 7.44 (t, *J* = 7.2 Hz, 2 H), 7.35 (b, 3 H), 7.29-7.21 (m, 4 H), 6.99 (d, *J* = 7.6 Hz, 1H), 6.90 (t, *J* = 6.4 Hz, 1 H), 6.73-6.69 (m, 5 H), 6.17 (s, 1 H), 2.30 (s, 6 H), 1.82 (s, 18 H); ^{13}C NMR (100 MHz, $CDCl_3$): δ (ppm) 158.59, 148.43, 147.83, 147.69, 147.07, 146.95, 145.25, 144.35, 142.29, 142.07, 141.98, 141.91, 141.03, 140.81, 140.60, 137.50, 137.17, 136.25, 134.75, 133.70, 132.56, 132.30, 131.64, 131.61, 131.54, 131.19, 131.08, 129.82, 129.39, 129.30, 128.92, 128.81, 128.52, 128.39, 127.68,

125.47, 125.37, 124.30, 124.15, 124.04, 123.17, 123.08, 122.22, 121.81, 121.29, 121.19, 119.58, 118.78, 100.52, 28.83, 28.70, 23.41, 21.24; ^{31}P NMR (162 MHz, $CDCl_3$): δ (ppm) 33.60; FAB-MS (*m/z*): 1069 $[M+Na]^+$; Anal. Calcd. for $C_{57}H_{51}BIrN_2O_3P$: C, 65.45; H, 4.91; N, 2.68; found: C, 65.39; H, 4.93; N, 2.59%.

X-ray Crystallography. Single crystal of **Ir-PON** (CCDC-1436827) was obtained by slow diffusion of its solution in $CHCl_3$ into hexane. The crystal was mounted in thin glass fiber and the data were collected on a Bruker SMART CCD diffractometer (Mo Kα radiation and λ = 0.71073 Å) in Φ and ω scan modes at 298 K. The structure was solved by direct methods followed by difference Fourier syntheses and then refined by full-matrix least-squares techniques against F^2 using *SHELXL-97* program on a personal computer.[36]

Computational Details. DFT calculations using B3LYP were performed for all of the iridium(III) complexes. The basis set used for C, H, N, O, P, S and B atoms was 6-31G (d, p), while effective core potentials with a LanL2DZ basis set were employed for Ir atoms.[37-38] The excitation behaviors of the complexes were computed by the TD-DFT method based on optimized geometries at the ground states. Additionally, UB3LYP was used to optimize the first triplet state (T_1) geometries and the natural transition orbital (NTO) was analyzed for $S_0 \rightarrow T_1$ excitation. All calculations were carried out by using the *Gaussian 09* program.[39]

OLED Fabrication and Measurements. The precleaned ITO (indium−tin oxide) glass substrates were treated with ozone for 20 min before poly(3,4-ethylenedioxythiophene): poly(styrene sulfonate) (PEDOT:PSS) was spin-coated on the surface of ITO glass substrates to form a 40-nm-thick hole-injection layer. Then, the ITO glass substrates with a PEDOT:PSS layer were cured at 120 °C for 30 min in air. The emission layer (40∼60 nm) was obtained by spin coating a solution of **Ir-PON**, **Ir-POO**, or **Ir-POB** and 4,4'-*N*,*N*-'dicarbazole-biphenyl

(CBP) in dichloromethane at various concentrations. The obtained ITO chip was dried in a vacuum oven at 70 °C for 30 min, and it was transferred to the deposition system for organic and metal deposition. 1,3,5-*tris*[*N*-(phenyl)-benzimidazole]-benzene (TPBi, 40 nm), LiF (1 nm), and Al cathode (100 nm) were successively deposited at a base pressure of less than 10^{-6} Torr. For each device, four pixels with the same device configuration were prepared at one batch and the deposited Al cathode overlaps with the precoated ITO anode to form an active area of 3×4 mm^2 for each pixel. The EL spectra and CIE coordinates were recorded with a PR650 spectra colorimeter. The *L*−*V*−*J* curves of the devices were measured by a Keithley 2400/2000 source meter, and the luminance was measured using a PR650 SpectraScan spectrometer for all four pixels. All of the experiments and measurements were carried out under ambient conditions.

RESULT AND DISCUSSION

Synthetic Strategies and Structural Characterization. Detailed synthetic protocols and relevant chemical structures are illustrated in **Scheme 1** and **Scheme 2**. Suzuki cross-coupling of 2-bromopyridine with (4-bromophenyl)boronic acid gave the compound **1**. Through lithiation in anhydrous THF at -78 °C and subsequent treatment with an excessive amount of trimethyl borate, compound **1** was converted into the boronic acid derivative compound **2**, which underwent another step of Suzuki cross-coupling with 1,2-dibromobenzene to afford compound **3** with the 2-bromo-1,1'-biphenyl unit for constructing PhFlPO moiety. Then, ligand **L-PO** had been synthesized according the literature with compound **3** as the starting material.[40] Metalation of the corresponding cyclometalating ligand (**L-N**/**L-O**/**L-B**) and ligand **L-PO** with $IrCl_3 \cdot nH_2O$ gave the cyclometalated Ir^{III} μ-chloro-bridged dimers, which were then converted into the target asymmetric *tris*-heteroleptic Ir^{III} complexes by reaction with thallium(I) acetylacetonate

[Tl(acac)].

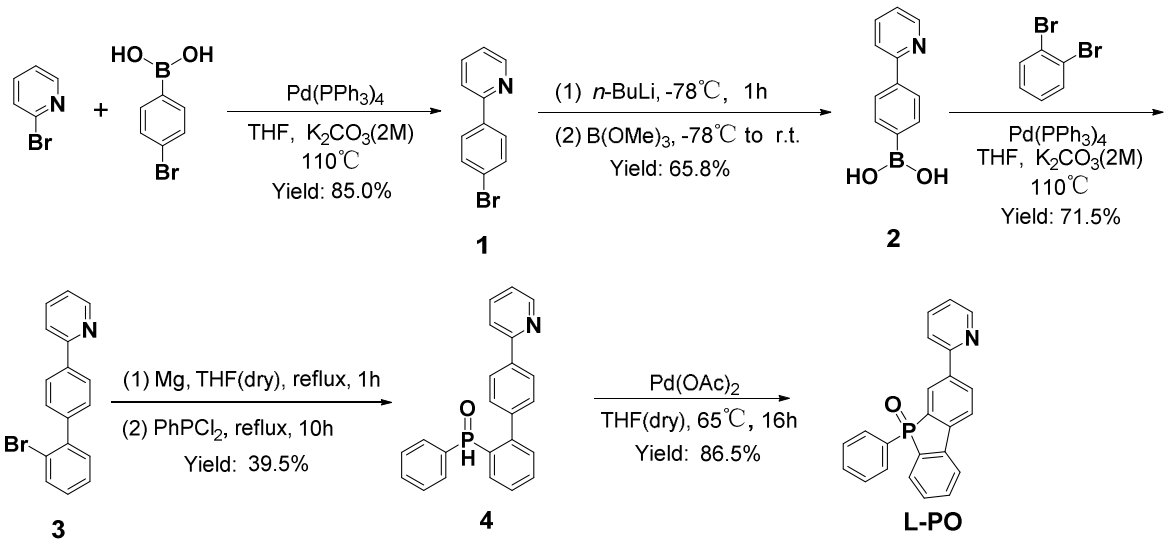

Scheme 1. Synthesis of ligand **L-PO**.

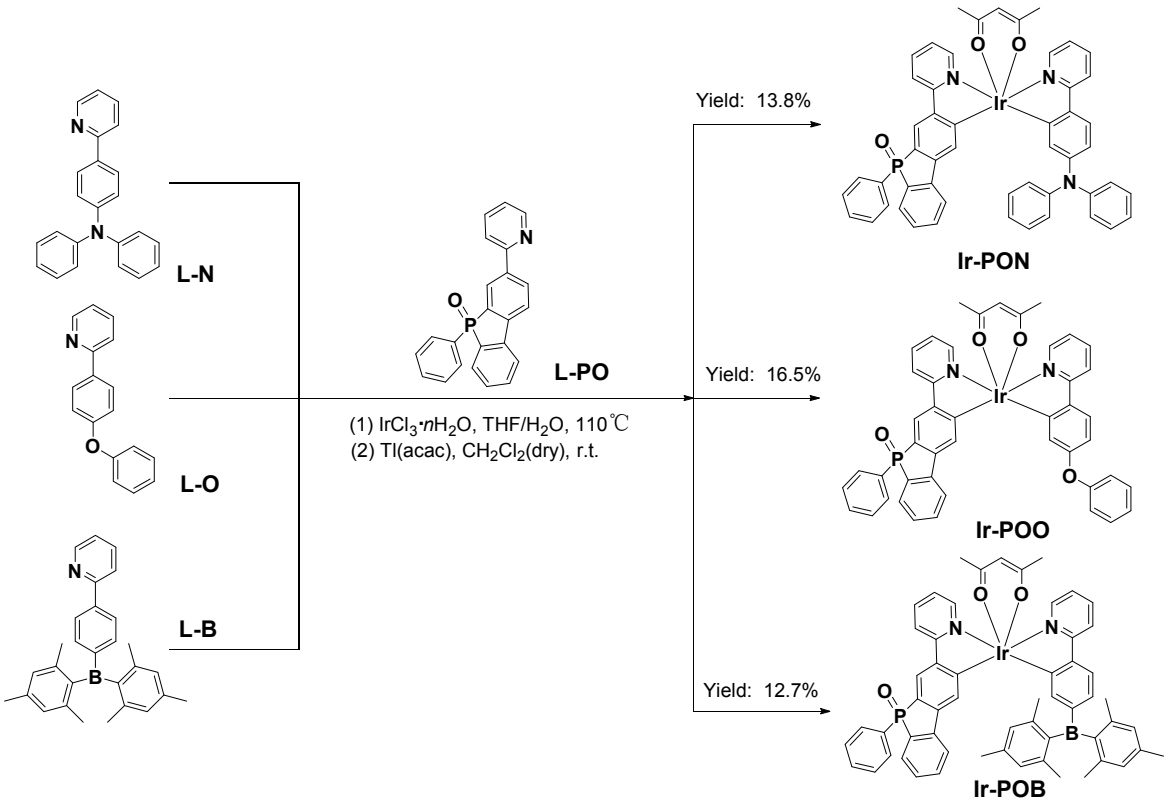

Scheme 2. Synthesis of the asymmetric *tris*-heteroleptic Ir^{III} complexes.

The chemical structures of these asymmetric *tris*-heteroleptic Ir^{III} complexes were fully

characterized by NMR spectra, including ^{1}H, ^{13}C and ^{31}P (**Figure S5**). In their ^{1}H-NMR spectra, they all show two sets of double resonance peak with the chemical shift at *ca.* 8.4-8.6 ppm and 8.2-8.4 ppm, respectively, which can be asigned to the two H atoms attached to the C atoms adjacent to the N atoms in the pyridine rings of the ligand **L-PO** and cooresponding **L-N**/**L-O**/**L-B**, respectively. In addition, in the ^{1}H-NMR spectra of **Ir-PON** and **Ir-POO**, the H atoms on the two methyl groups in the acethylacetone (Hacac) auxillary ligands split into two sets of single resonance peak with the chemical shifts at *ca.*1.80 ppm and 1.84 ppm, respectivley. On contrary, only one set of double resonance peak was found for these H atoms for the traditonal *bis*-heteroleptic Ir^{III} complexes with two identical cyclometalating ligands.[41] The signals from the H atoms of the two methyl groups of the acethylacetone auxillary ligand of **Ir-POB** overlap with those of the four *o*-methyl groups of the $B(Mes)_2$ unit. In their ^{31}P-NMR spectra, the signals of the P atoms are found at *ca.* 34.0 ppm for all three Ir^{III} complesex. Combined the information from their ^{13}C-NMR spectra, the *tris*-heteroleptic structures of these Ir^{III} cyclometalated complexes have been fully comfirmed. Further more, the single crystal of **Ir-PON** was successfully prepared by slow diffusion of its solution in $CHCl_3$ into hexane and its structure has been investigated by single-crystal X-ray crystallography. The ORTEP drawing of **Ir-PON** is illustrated in **Figure 1** and detailed structural data have been showed in **Table S1** and **Table S2** in Supporting Information (SI). As depicted in **Figure 1**, the coordination configuration around Ir center is a distorted octahedron with *cis*-O,O, *cis*-C,C, and *trans*-N,N chelating disposition. The bond length of the Ir-C, Ir-N and Ir-O bonds are similar with our previous result of *tris*-heteroleptic Ir^{III} complexes.[17-18] The phosphafluorene moiety in ligand **L-PO** can show good planar geometry, while the C(10)-P(1), C(17)-P(1), C(18)-P(1) and the P(1)-O(1) bonds form a distorted tetrahedral configuration with the bond angles around the P

atom ranging from 92.9 to 116.8º (**Table S1**). The three C-P bonds have similar bond length *ca.* 1.80 Å and the P(1)-O(1) bond have a bond length of *ca.* 1.45 Å (**Table S1**). The pendant phenyl ring and the P(1)-O(1) bond are out of the phosphafluorene plane (**Figure 1**).

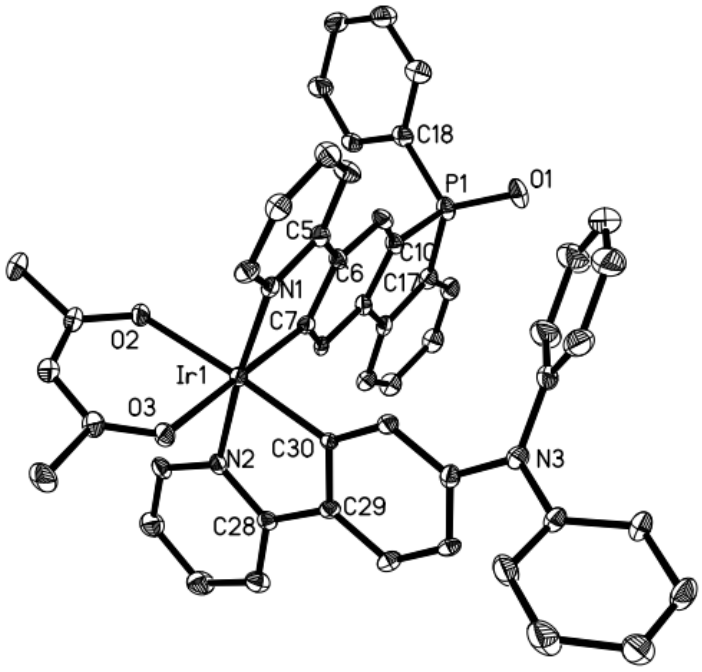

Figure 1. ORTEP drawing of **Ir-PON** with thermal ellipsoids drawn at the 10% probability level. The H atoms are omitted for clarity.

Thermal and Photophysical Properties. Thermogravimetric analysis (TGA) and differential scanning calorimetry (DSC) (both under a nitrogen flow) were to characterized the thermal properties of these Ir^{III} complexes. All three Ir^{III} complexes show good thermal stability with their 5% weight-reduction temperature ($\Delta T_{5\%}$) ranging from 357-365 °C. The DSC traces reveal a high glass transition temperature (T_g) of *ca.* 150 °C for these Ir^{III} complexes, which should be attributed to the branched and distorted configuration of the PhFlPO moiety and the OPh, NPh_2 and $B(Mes)_2$ group. The high thermal stability of these Ir^{III} complexes is sufficient for the fabrication of OLEDs with solution-process technique. Two major absorption bands have been found in the UV/Vis absorption spectra of these asymmetric *tris*-heteroleptic Ir^{III} complexes

(**Figure 2a**). According to the literature, the intense absorption bands located in high energy region (<330 nm for **Ir-POO** and **Ir-PON**, and <400 nm for **Ir-PON**, respectively) could be safely ascribed to the spin-allowed $^1\pi\rightarrow\pi^*$ transitions of the cyclometalating ligands, whereas the much weaker absorption bands extended to the visible light region were tentatively assigned to the excitation to both singlet and triplet MLCT states (MLCT = metal-to-ligand charge transfer).[41] The excitation to the LLCT and/or ILCT (ILCT = intra-ligand charge transfer, LLCT = ligand-to-ligand charge transfer) states might also contribute to these low-energy absorption bands to some extent (*vide infra*). The photoluminescence (PL) spectra (**Figure 2b**) of these Ir^{III} complexes at 293 K have been collected under excitation at 400 nm. All three complexes exhibited intense phosphorescent emission, substantiated by their relatively short phosphorescent lifetime (τ_p, **Table 1**) and prolonged τ_p at 77K (2.98 μs, 2.57 μs and 3.39 μs for **Ir-PON**, **Ir-POO** and **Ir-POB**, respectively). **Ir-POB** displays a broad and structureless PL spectrum with emission maximum (λ_{em}) located at *ca.* 588 nm, indicating the predominant ^{3}MLCT character of its lowest triplet excited states.[41] However, the PL spectra for **Ir-PON** and **Ir-POO** are well-structured with λ_{em} found at *ca.* 549 nm and *ca.* 544 nm, respectively, accompanied by an emission shoulder at *ca.* 591 nm and *ca.* 588 nm, respectively. Upon cooling to 77K, the PL spectra of these complexes in CH_2C_2 became more resolved (**Figure S1**). Apart from the emission peaks observed in the room-temperature PL spectra, an additional emission peak centered at *ca.* 650 nm arises for **Ir-PON** and **Ir-POO**, and *ca.* 630 nm for **Ir-POB** (**Table 1**), respectively. The well-defined vibronic structure of their PL spectra indicates that the ^{3}ILCT/^{3}LLCT states may be substantially involved in the radiative decay of the lowest triplet excited states of **Ir-PON** and **Ir-POO** in addition to the ^{3}MLCT excited states. Similar to our previously results,[16-18] the emission maxima of **Ir-PON** and **Ir-POO** have been red-shifted upon

replacing one of the cyclometalating ligands of the traditional *bis*-heteroleptic Ir^{III} complexes with ligand **L-PO** (λ_{em}: **Ir-N** *ca.* 533 nm and **Ir-O** *ca.* 505 nm, **Figure S2** and **Table S3**) whereas the λ_{em} of **Ir-POB** exhibits a hypsochromic shift compared with that of the *bis*-heteroleptic counterpart **Ir-B** (*ca.* 605 nm, **Figure S2** and **Table S3**) (*vide infra*).

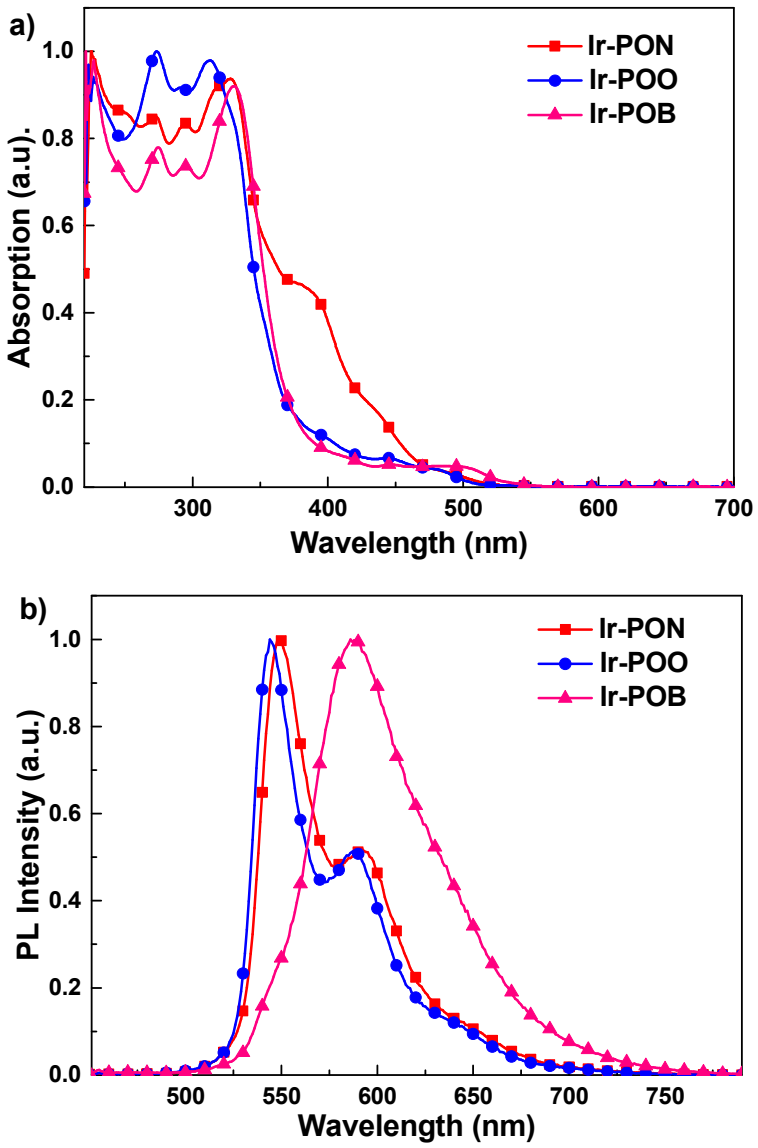

Figure 2. a) UV/Vis and b) PL spectra of the asymmetric *tris*-heteroleptic Ir^{III} complexes in CH_2Cl_2 at 293 K.

Table 1 Photophysical data of the asymmetric *tris*-heteroleptic Ir^{III} complexes.

Complexes	λ_{abs} (nm) (293 K)[a]	λ_{em} (nm)[b] 293K/77K	Φ_p[b] solution/film	τ_p[c] (μs) 293K/77K	τ_r[d] (μs)	$\Delta T_{5\%}/T_g$[e] (°C)
Ir-PON	225 (5.08), 251 (5.02), 271 (5.01), 295 (5.01), 318 (5.05), 328 (5.06), 392 (4.72), 440 (4.29), 497 (3.56)	549, 591[sh] /550, 596[sh]	0.39 /0.42	1.05 /2.98	2.69	363/151
Ir-POO	227 (4.99), 273 (5.02), 292 (4.98), 314 (5.01), 399 (4.07), 445 (3.84), 484 (3.60)	544, 588[sh] /546, 593[sh]	0.62 /0.56	1.24 /2.57	2.00	357/149
Ir-POB	227 (5.16), 274 (5.06), 295 (5.03), 331 (5.13), 416 (3.99), 446 (3.88), 505 (3.81)	588 /583, 626[sh]	0.40/ 0.46	1.12 /3.39	2.80	365/153

[a] Measured in CH_2Cl_2 at a concentration of 10^{-5} M, and log ε values are shown in parentheses. sh: Shoulder [b] In CH_2Cl_2 solution relative to *fac*-[Ir(ppy)$_3$] (Φ_p = 0.40) with λ_{ex} = 400 nm and 8 wt.-% of Ir^{III} complexes doped CBP film with λ_{ex} = 365 nm. [c] Measured in degassed CH_2Cl_2 solutions at a concentration of *ca.*10^{-5} M with a 370 nm excitation source at 293 K and 77K. [d] The triplet radiative lifetimes (τ_r) were deduced from $\tau_r = \tau_P/\Phi_P$. [e] $\Delta T_{5\%}$ represents for the 5% weight-reduction temperature and T_g is the glass transition temperature.

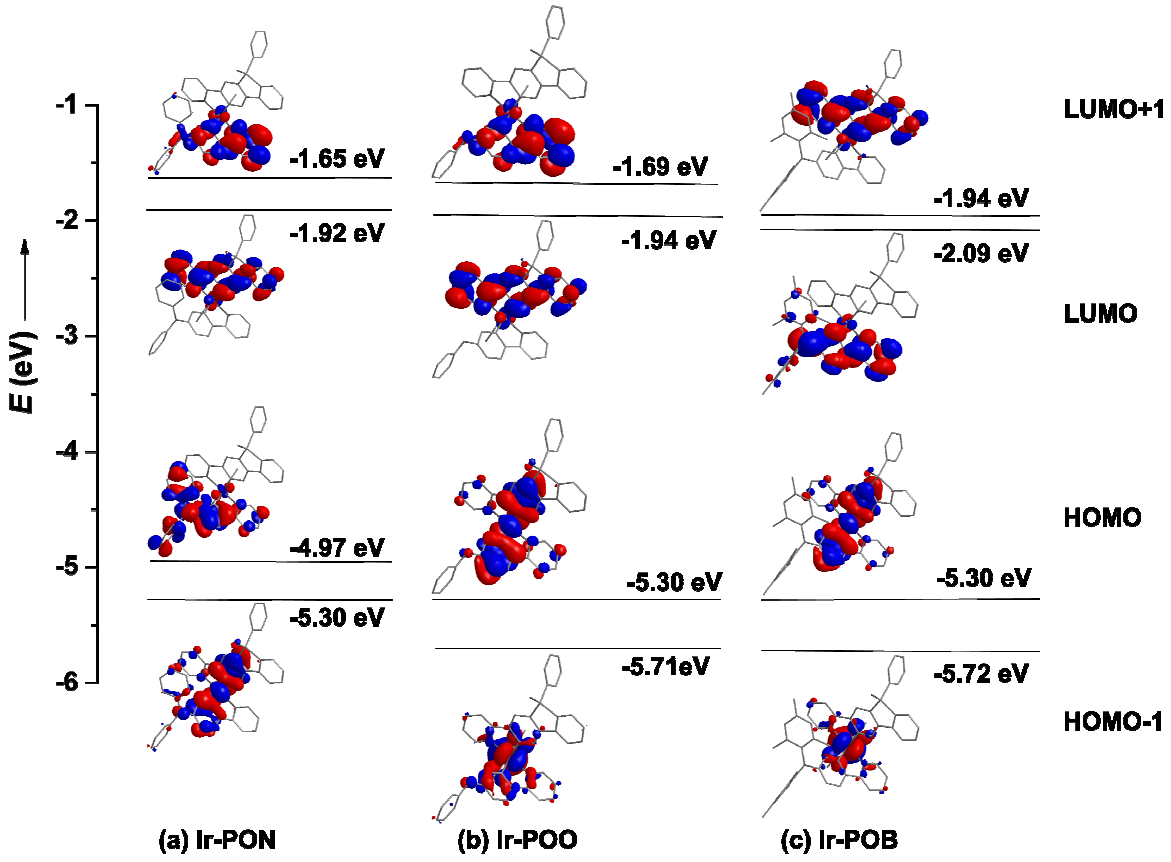

Figure 3. Molecular orbital patterns (isocontour value=0.025) for the asymmetric *tris*-heteroleptic Ir^{III} complexes based on their optimized S_0 geometries

Table 2. TD-DFT results for *tris*-heteroleptic Ir^{III} Complexes based on their optimized S_0 geometries

Complexes	MO	Contribution percentages of metal d_π orbitals and π orbitals of ligands to MOs/%				Main configuration of $S_0 \rightarrow S_1$ excitation /E_{cal}/λ_{cal}/f [a]	Main configuration of $S_0 \rightarrow T_1$ excitation /E_{cal}/λ_{cal} [a]
		Ir	**L-N**	**L-PO**	**acac**		
Ir-PON	L+1	3.91	94.43	0.95	0.71	H→L (89.35%)	H→L+1 (74.55%)
	L	3.32	0.79	95.37	0.52	2.569 eV	2.316 eV
	H	2.83	96.25	0.78	0.14	482.6 nm	535.4 nm
	H-1	41.82	26.32	26.80	5.06	0.0071	
		Ir	**L-O**	**L-PO**	**acac**		
Ir-POO	L+1	4.13	94.21	0.86	0.81	H→L (94.48%)	H→L (72.93%)
	L	3.33	0.69	95.45	0.53	2.693 eV	2.364 eV
	H	39.95	30.44	25.49	4.12	460.4 nm	524.6 nm
	H-1	34.20	13.97	7.68	44.16	0.0273	
		Ir	**L-B**	**L-PO**	**acac**		
Ir-POB	L+1	3.33	2.01	94.06	0.60	H→L (95.28%)	H→L (87.36%)
	L	2.33	95.51	1.76	0.39	2.555 eV	2.258 eV
	H	42.65	27.47	25.35	4.52	485.3 nm	549.0 nm
	H-1	37.63	5.67	5.46	51.24	0.0309	

[a] H→L represents the HOMO to LUMO transition. E_{cal}, λ_{cal} and f represents for calculated excitation energy, calculated absorption wavelength and oscillator strength respectively. The oscillator strength of $S_0 \rightarrow T_1$ excitation is zero due to the spin-forbidden of singlet-triplet transition under TD-DFT calculation in Gaussian program without considering the spin-orbit coupling.

Time-dependent density functional theory (TD-DFT) calculations have been carried out to gain insight into the photophysical behaviors of these asymmetric *tris*-heteroleptic Ir^{III} complexes. **Figure 3** displays the distribution patterns of the highest occupied molecular orbital (HOMO), the lowest unoccupied molecular orbital (LUMO), HOMO-1 and LUMO+1. Detailed TD-DFT results for these Ir^{III} complexes are listed in **Table 2**. The large contribution of HOMO→LUMO transitions to the $S_0 \rightarrow S_1$ transitions indicates that the frontier molecular

orbitals (FMOs) can represent the characters the lowest singlet excited states (S_1). Normally, for the conventional *bis*-heteroleptic Ir^{III} complexes incorporating ppy-type cyclometalating ligands, their HOMOs consist primarily an admixture of the π orbitals of two phenyl rings directly coordinated with the Ir center and the d_π orbital of Ir center, whereas their LUMOs are mainly located on the two pyridine rings. Therefore, the T_1 states of these complexes possess a ^{3}MLCT-dominated characteristic, substantiated by their structureless room-temperature PL spectra.[16]

As illustrated in **Figure 3**, the HOMO and LUMO distribution patterns of these asymmetric *tris*-heteroleptic Ir^{III} complexes are distinctively different from both that of traditional *bis*-heteroleptic Ir^{III} complexes and that of the each other.[16] For **Ir-PON**, its LUMO is predominately located on ligand **L-PO** (95.37%, **Table 2**) with substantial contribution from both the pyridine ring and the phosphafluorene moiety. As for its HOMO, it consists of a major contribution from ligand **L-N** (96.25%, **Table 2**) accompanied with a minor contribution from both the pyridine ring of ligand **L-N** and the d_π orbitals of Ir center (*ca.* 2.83%). The unusual low contribution of the d_π orbitals of Ir center in **Ir-PON** to its HOMO may result from the strong electron-donating property of the NPh_3 moiety excluding the participation of Ir center in the HOMO, which has also been observed for other Ir^{III} complexes incorporating NPh_3 moiety.[42] Therefore, the low-energy absorption bands in the UV/Vis absorption spectrum of **Ir-PON** should be mainly assigned to the LLCT (ligand **L-N** → ligand **L-PO**) transitions rather than MLCT transitions considering the minor contribution of d_π orbitals of Ir center to its HOMO. For **Ir-POO**, its LUMO pattern is quite similar with that of **Ir-PON** with the predominant contribution from ligand **L-PO** (95.45%, **Table 2**). However, distinct differences are found

between HOMOs of **Ir-POO** and **Ir-PON**. In contrast with the situation in **Ir-PON**, the d_π orbital of Ir center in **Ir-POO** gives a substantial contribution (*ca.* 39.95%) to its HOMO. The two phenyl rings directly chelated to the Ir center also constitute a major proportion of the HOMO of **Ir-POO**. Meanwhile, the TD-DFT results show that the H → L transition also contributes the largest proportion to the S_1 state of **Ir-POO**. Therefore, the low-energy absorption bands in the UV/Vis absorption spectrum of **Ir-POO** should be assigned to an admixture of MLCT, LLCT (ligand **L-O** → ligand **L-PO**) transitions. As for **Ir-POB**, on one hand, its HOMO pattern is similar to that of **Ir-POO** with contribution from both d_π orbital of Ir center (*ca.* 42.65%) and π orbitals of the two phenyl rings coordinated with Ir center. On the other hand, its LUMO distribution pattern is different from that of both **Ir-PON** and **Ir-POO**, showing ligand **L-B**-dominated characteristic (95.51%, **Table 2**) with a substantial contribution from the "empty" p_π orbital of boron atom of the $B(Mes)_2$ moiety. The LUMO pattern of **Ir-POB** actually resembles the LUMO distribution pattern of its *bis*-heteroleptic counterpart **Ir-B**.[16] Therefore, the low-energy absorption bands in the UV/Vis absorption spectrum of **Ir-POB** consist of an admixture of MLCT, LLCT (ligand **L-PO** → ligand **L-B**) transitions. For **Ir-POO** and **Ir-POB**, local excitation should also be involved in their UV/Vis absorption considering the considerable contributions from ligand **L-PO** (25.49%) and **L-B** (27.47%) to their HOMOs, respectively, which accounts for the substantially higher oscillator strength (**Table 2**) of $S_0 \rightarrow S_1$ excitation for **Ir-POO** and **Ir-POB** than that of **Ir-PON**.[43]

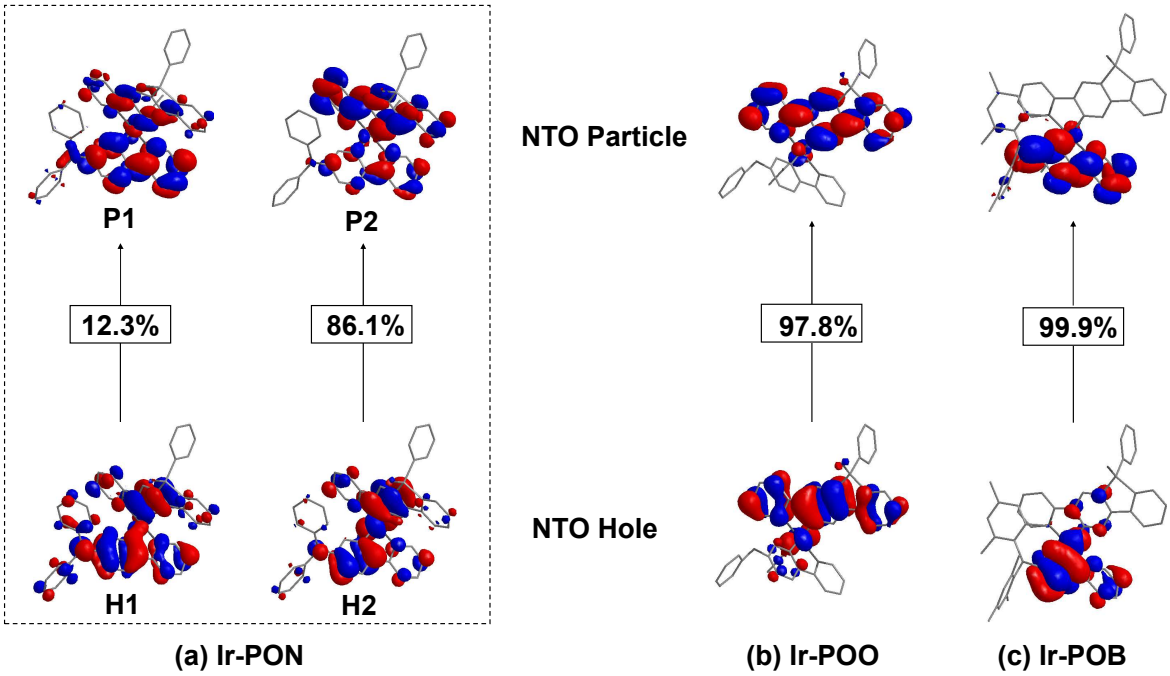

Figure 4 Natural transition orbital patterns (isocontour value=0.025) for $S_0 \rightarrow T_1$ excitation for the asymmetric *tris*-heteroleptic Ir^{III} complexes based on their optimized T_1 geometries

Table 3 NTO results for *tris*-heteroleptic Ir^{III} Complexes based on their optimized T_1 geometries

Complexes	NTO [a]	Contribution percentages of metal d_π orbitals and π orbitals of ligands to NTOs /%			
		Ir	**L-N**	**L-PO**	**acac**
	H1	3.73	61.90	33.88	0.49
Ir-PON	P1	4.15	70.58	24.78	0.49
	H2	27.23	37.13	33.27	2.37
	P2	3.70	25.53	70.20	0.57
		Ir	**L-O**	**L-PO**	**acac**
Ir-POO	H	18.53	4.50	75.69	1.28
	P	3.94	0.43	95.09	0.54
		Ir	**L-B**	**L-PO**	**acac**
Ir-POB	H	32.29	56.01	8.68	3.02
	P	3.83	95.05	0.55	0.58

[a] H and P represents for NTO hole and particle orbital, respectively.

With regard to the T_1 state of these *tris*-heteroleptic Ir^{III} complexes, natural transition orbital (NTO) analysis was carried out for the $S_0 \rightarrow T_1$ excitation using the optimized T_1 geometries of these asymmetric *tris*-heteroleptic Ir^{III} complexes (**Figure 4**) and we will focus on the NTO results (**Table 3**) to elucidate the photoluminescent behaviors of these asymmetric *tris*-heteroleptic Ir^{III} complexes. The NTO analysis gave out two pairs of hole to particle transitions for **Ir-PON** with the contribution percentage of 12.3% and 86.1%, respectively (**Figure 4a**). For the H1→P1 transition (12.3%), both its hole and particle orbitals are strongly localized on ligand **L-N** (61.90% and 70.58%, respectively) and **L-PO** (33.88% and 24.78%, respectively) with negligible fraction on the d_π orbital of Ir center (3.73% and 4.15%, respectively). Therefore, the H1→P1 transition should be an ILCT-dominated process. For the H2→P2 transition (86.1%), its hole orbital is delocalized on ligand **L-N** (37.13%), d_π orbital of Ir center (27.23%) and ligand **L-PO** (33.27%) while its particle orbital is mainly localized on ligand **L-PO** (70.20%) with a minor fraction on ligand **L-N** (25.53%), manifesting a MLCT/LLCT character for H2→P2 transition. As one can see from the distribution patterns of NTO hole and particle orbitals for **Ir-PON**, they all display a prevailing ligand-centered character. Therefore, taking the contribution percentages of these two pairs of NTO transitions into account, we can conclude that the ^{3}ILCT/^{3}LLCT dominate the character of the T_1 state of **Ir-PON** while the ^{3}MLCT transition takes the secondary place. This kind of assignment is further corroborated by the well-structured PL spectrum for **Ir-PON**.[41] Replacing one of the NPh_3 moiety in traditional *bis*-heteroleptic **Ir-N** with electron-withdrawing PhFlPO moiety would form a donor-acceptor (D-A) structure within the resulting asymmetric *tris*-heteroleptic **Ir-PON**. Obviously, the presence of the D-A structure within **Ir-PON** will facilitate the charge transfer transitions in the excitation and radiative decay processes.[44] Consequently, **Ir-PON**

exhibit a red-shift of both its low-energy absorption bands and the λ_{em} compared with those of its *bis*-heteroleptic counterparts (**Figure S2** and **Table S3**).[16]

As for **Ir-POO**, the NTO analysis for **Ir-POO** shows that its hole orbital is mainly located on ligand **L-PO** (75.69%) and the d_π orbital of the Ir center (18.53%) while the particle orbital is strongly localized on ligand **L-PO** (95.09%, **Figure 4b**). Therefore, the NTO results suggest that the T_1 state of **Ir-POO** has a ^{3}ILCT-dominated (Ligand **L-PO**) character with ^{3}MLCT at a subordinate position. The substantial involvement of the ligand-centered charge transfer transition processes in the radiative decay of the T_1 states is corroborated by the well-structured PL spectrum, compared with that of its *bis*-heteroleptic counterpart **Ir-O** (**Figure S2** and **Table S3**).[16] Compared the NTO results of **Ir-POO** with those of **Ir-PON**, a great extent of similarity could be seen here that the ligand-centered character outweighs that of MLCT for their T_1 states, eventuating in the significant similarities between the PL spectra of **Ir-PON** and **Ir-PON** (**Figure 2b** and **Table 1**). So, both **Ir-POO** and **Ir-PON** exhibit similar well-structured phosphorescent emission spectra (**Figure 2b**). Same as **Ir-PON**, the incorporating of electron-withdrawing PhFlPO moiety also forms a D-A structure within **Ir-POO** to red-shift both its low-energy absorption bands and λ_{em} (**Table 1**) with respect to the *bis*-heteroleptic counterpart **Ir-O**.[16,44] Owing to the much weaker electron-donating property of OPh unit than that of NPh_2 unit, **Ir-POO** emits at a shorter wavelength compared with **Ir-PON**.

The NTO analysis for **Ir-POB** (**Figure 4** and **Table 3**) shows that its hole orbital is mainly located on the d_π orbital of the Ir center (32.29%) and ligand **L-B** (56.01%) whereas its particle orbital is strongly localized on ligand **L-B** (95.05%). A prevailing character of ^{3}MLCT in the T_1 state of **Ir-POB** can be clearly seen, which is confirmed by the structureless shape of the PL

spectrum for **Ir-POB** at room temperature (**Figure 2b**). Our previously investigation of the photophysical on corresponding *bis*-heteroleptic **Ir-B** have shown that the electrons in the MLCT processes are primarily directed to the $B(Mes)_2$ moiety rather than the pyridine rings because of the strong electron-accepting property of $B(Mes)_2$ moiety[16], a situation which still holds for the *tris*-heteroleptic **Ir-POB** considering the large contribution from the "empty" p_π orbital of boron atom in its NTO particle orbital. However, the strong electron-withdrawing PhFlPO moiety will make the electrons from both PhFlPO moiety and Ir center more reluctant to be transferred to the $B(Mes)_2$ moiety and consequently impede the MLCT processes, causing destabilization of MLCT states. As results, the low-energy absorption bands and the λ_{em} of **Ir-POB** are shifted to shorter emission wavelength compared with those of the *bis*-heteroleptic counterpart **Ir-B** (**Figure S2** and **Table S3**).[16] Despite of the negative influence from the PhFlPO unit, the strong electron-accepting ability of the $B(Mes)_2$ moiety still can furnish more stabilized MLCT states in **Ir-POB** than those in both **Ir-PON** and **Ir-POO**, indicated by its red-shifted low-energy absorption bands with respect to that of **Ir-PON** and **Ir-POO** (**Figure 2**). Hence, **Ir-POB** can emit phosphorescence with much longer wavelength than **Ir-PON** and **Ir-POO**.

Generally, the $T_1 \rightarrow S_0$ transitions (phosphorescent emission) are spin-forbidden. This kind of restriction can be partially alleviated by mixing the T_1 excited states with the high-lying singlet (S_n) excited states, a process triggered by the spin-orbit coupling (SOC). Despite of that, the phosphorescence of pure organic materials is still very weak and most of them can only be detected at very low temperature due to the weak SOC effect associate with these materials. However, the strong SOC effect associated with transition heavy metal atom (especially Ru^{II}, Os^{II}, Ir^{III} and Pt^{II})[45] can greatly promote the mixing between T_1 and S_n states and facilitate

efficient intersystem crossing (ISC) from singlet excited states to triplet excited states. Consequently, the complexes incorporating these transitions heavy metal center exhibit intense room-temperature phosphorescent emission with high phosphorescent quantum yields (Φ_p) and substantially shortened τ_p compared with pure organic materials. The Φ_p of these *tris*-heteroleptic Ir^{III} complexes in degassed CH_2Cl_2 solution have been measured using *fac*-$Ir(ppy)_3$ as the reference with 0.39, 0.62 and 0.40 for **Ir-PON**, **Ir-POO** and **Ir-POB**, respectively (**Table 1**). Additional, their Φ_p in CBP films were also measured in integrating sphere (**Table 1**). The doping ratio was 8 wt.-% for all three complexes. All three complexes showed comparable Φ_p in film to those of their solution with 0.42, 0.56 and 0.46 for **Ir-PON**, **Ir-POO** and **Ir-POB**, respectively. Attributed to the some MLCT character in the T_1 states of **Ir-PON** and **Ir-POO**, their T_1 states were effectively mixed with the high-lying singlet states, facilitating efficient phosphorescent emission.[44] Despite of the dominating character of MLCT in the T_1 state of **Ir-POB**, it only gave out moderate Φ_p (both in solution and film), a situation induced by the band-gap law that emitters with longer emission wavelength tend to be less luminescent.[46] The τ_p of these complexes is in the order of *ca.* one microsecond (μs) (**Table 1**), typically observed in ppy-type Ir^{III} phosphorescent complexes.

Electrochemical Properties. The cyclic voltammetry (CV) had been performed with ferrocene as the internal standard to investigate the electrochemical properties of these asymmetric *tris*-heteroleptic Ir^{III} complexes. During the anodic scans, all the three complexes exhibit a reversible oxidation process at *ca.* 0.5 V (0.45 V for **Ir-PON**, 0.53 V for **Ir-POO** and 0.55 V for **Ir-POB**), which can be assigned to the oxidation of the Ir center (**Table 4**). Compared with their symmetric *bis*-heteroleptic counterparts,[16] these asymmetric *tris*-heteroleptic complexes show

higher oxidation potentials for the Ir centers, which should be induced by the strong electron-withdrawing PhFlPO moiety for efficiently lowering the electron density on the Ir centers. Owing to the electron-donating main-group moieties OPh and NPh_2 which can provide electron density to the Ir center, **Ir-PON** (*ca.* 0.45 V) and **Ir-POO** (*ca.* 0.53 V) possess lower oxidation potentials for their Ir centers than that for **Ir-POB** (*ca.* 0.55 V) bearing electron-withdrawing PhFlPO moiety and electron-accepting $B(Mes)_2$ unit (**Table 4**). Besides the oxidation potential for Ir center, **Ir-PON** and **Ir-POO** also display another oxidation wave at lower potential of *ca.* 0.38 V and 0.42 V, respectively (**Table 4**). This can be ascribed to the oxidation of electron-donating main-group moieties OPh and NPh_2.[17-18]

Multiple reduction processes have been observed for these asymmetric *tris*-heteroleptic Ir^{III} complexes. They all possess a reduction peak located in the range from *ca.* −2.30 V to −2.40 V, which can be ascribed to the reduction of main-group PhFlPO moiety.[46] The reduction peaks at much lower potential (*ca.* −2.67 V for **Ir-PON**, *ca.* −2.62 V for **Ir-POO** and *ca.* −2.75 V, −2.85 V for **Ir-POB**) can be assigned to the reduction of the pyridine rings in the organic ligands (**Table 4**). Based on our previously results,[24] the reduction peak at *ca.* −2.12 V of **Ir-POB** should be induced by the reduction of the main-group $B(Mes)_2$ moiety in ligand **L-B**, while the reduction peak at *ca.* −2.43 V comes from the reduction of PhFlPO moiety. Due to the existence of both strong electron-accepting $B(Mes)_2$ moiety and electron-withdrawing PhFlPO group, the reductions of pyridine rings in **Ir-POB** have been shifted to much more negative potentials (*ca.* −2.75 V and *ca.* −2.85 V). The LUMO levels of these complexes range from *ca.* −2.49 eV to *ca.* −2.68 eV, which are significantly lower than those of their *bis*-heteroleptic counterparts.[16] The substantially lower LUMO levels will definitely enhance the EI/ET abilities of these asymmetric *tris*-heteroleptic Ir^{III} complexes.

Table 4. Redox properties of the asymmetric *tris*-heteroleptic Ir^{III} complexes.

Complex	$E_{1/2}^{ox}$ (V)		$E_{1/2}^{red}$ (V)		HOMO (eV)	LUMO (eV)
	Main-group moiety	Metal center	Main-group moiety	Pyridyl moiety		
Ir-PON	0.38	0.45	–2.27	–2.67	–5.18	–2.53
Ir-POO	0.42	0.53	–2.30	–2.62	–5.22	–2.50
Ir-POB		0.55	–2.12, –2.43	–2.75, –2.85	–5.35	–2.68

As aforementioned, the superior EI/ET properties of the cyclometalated phosphorescent emitters are very crucial to gain balanced charge carrier injection/transporting to further improve the EL performance of the concerned OLEDs. In addition, the electron-donating main-group moieties OPh and NPh_2 can furnish good HI/HT ability, which can bring forth ambipolar features through combining with the strong EI/ET properties from PhFlPO moiety. Therefore, the PhFlPO moiety can show great potential in conferring the concerned Ir^{III} complexes with excellent EI/ET properties and hence furnishing highly efficient OLEDs.

Charge Carrier Transporting Properties and Electrophosphorescent OLEDs. In order to verify the design concept that incorporating of PhFlPO moiety into the Ir^{III} complexes could confer EI/ET properties to the concerned Ir^{III} complexes, we fabricated the single carrier devices of these three asymmetric *tris*-heteroleptic Ir^{III} complexes both in neat films and doped into CBP at a doping ratio of 8 wt.-% and the famous *bis*-heteroleptic $Ir(ppy)_2(acac)$ as control (**Figure 5**).

For the hole-only devices of the neat films (**Figure 5a**), all three asymmetric *tris*-heteroleptic

Ir^{III} complexes show lower current density compared with that of the neat film of CBP. Besides, **Ir-PON** and **Ir-POO** show slightly higher hole-only current density than that of $Ir(ppy)_2(acac)$ where **Ir-POB** shows slightly lower hole-only current density than that of $Ir(ppy)_2(acac)$ (**Figure 5a**). The incorporation of electron-donating NPh_2 and OPh moiety should be the reason behind the higher hole-only current density of **Ir-PON** and **Ir-POO** than that of $Ir(ppy)_2(acac)$ under a given driving voltage. The lowest hole-only current density of **Ir-POB** among these three Ir^{III} complexes and lower than that of $Ir(ppy)_2(acac)$ should be the result of existence of both strong electron-accepting $B(Mes)_2$ moiety and electron-withdrawing PhFlPO group impeding the HI/HT process.

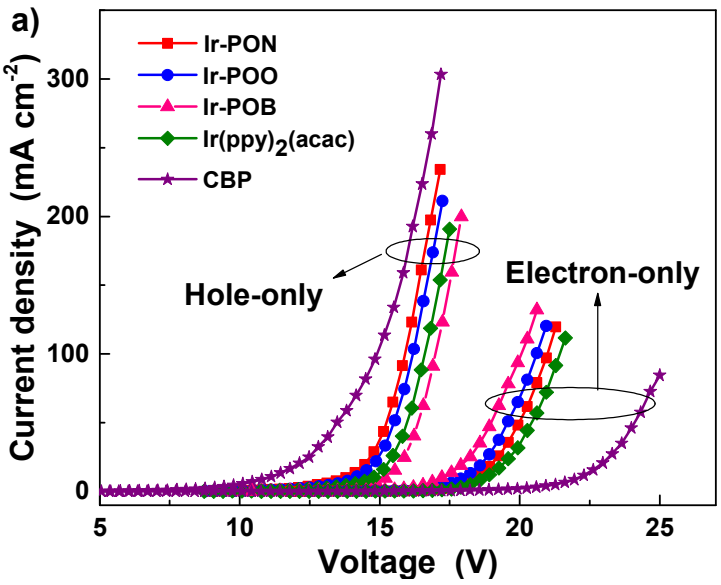

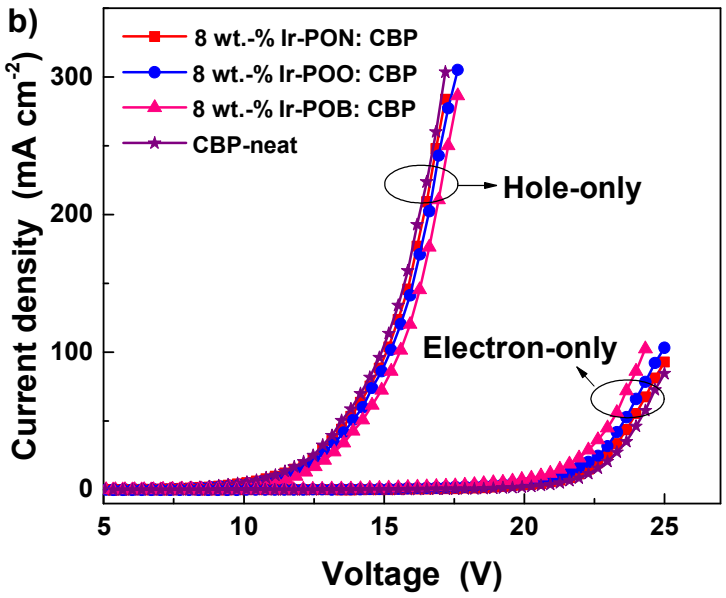

Figure 5. The Current Density-Voltage (*J-V*) curves for single carrier devices of a) neat and b) CBP film doped with 8 wt.-% of **Ir-PON**, **Ir-POO** and **Ir-POB**, and CBP-neat. Hole-only Device: ITO/MoO_3 (3 nm)/PEDOT: PSS (20 nm)/Active layer (50 nm)/PEDOT: PSS (20 nm)/MoO_3 (3 nm)/Al (100 nm); Electron-only Device: ITO/LiF (3 nm)/Active layer (50 nm)/LiF (3 nm)/Al (100 nm)

As for the electron-only devices of the neat films (**Figure 5a**), all three asymmetric *tris*-heteroleptic Ir^{III} complexes show remarkably higher current density than that of the neat film of CBP. Together with the high hole-only current density, it clearly demonstrates the ambipolar charge carrier transporting character of these three Ir^{III} complexes. The electron-only current of these three Ir^{III} complexes goes with the trend of **Ir-POB**>**Ir-POO**>**Ir-PON** and all three Ir^{III} complexes exhibit higher electron-only current density compared with that of $Ir(ppy)_2(acac)$ (**Figure 5a**), proving the feasibility of the strong electron-withdrawing PhFlPO moiety in conferring excellent EI/ET to the concerned Ir^{III} complexes. The combination of EI/ET groups of both $B(Mes)_2$ and PhFlPO greatly boosts the EI/ET ability of **Ir-POB** as indicated by its highest electron-only current among these three Ir^{III} complexes (**Figure 5a**). The best EI/ET property of **Ir-POB** among these three Ir^{III} complexes correlate well with the CV results that **Ir-POB** shows the lowest LUMO level of -2.68 eV (**Table 4**). After being doped into CBP at a doping ratio of 8

wt.-%, the current density of the hole-only and electron-only devices of these three Ir^{III} complexes are leveled to those of the neat film of CBP (**Figure 5b**), because of the low concentration of these Ir^{III} complexes in the CBP films. However, the electron-only current density of these three Ir^{III} complexes is still slightly higher than that of the neat film of CBP, indicating the excellent EI/ET of these Ir^{III} complexes.

To evaluate their EL potentials, these asymmetric *tris*-heteroleptic Ir^{III} complexes were used as dopants to construct OLEDs using solution process technique. The general configuration of these devices are ITO/PEDOT:PSS (40 nm)/Ir x%:CBP (40～60 nm)/TPBi (40nm)/LiF(1 nm)/Al (100nm) (**Figure 6**). The well-known CBP (4,4'-*N*,*N*'-dicarbazole-biphenyl) was used as the host material due to its dominantly hole-transporting properties. PEDOT:PSS (poly(3,4-ethylenedioxythiophene): poly(styrene sulfonate)) was used to facilitate hole injection from the anode to the emission layer (EML) and a layer of TPBi (1,3,5-*tris*[*N*-(phenyl)-benzimidazole]-benzene) was inserted to serve the function of both electron-transporting and hole-blocking. Variation of the doping levels has been carried out in order to optimize the EL performance of OLEDs.

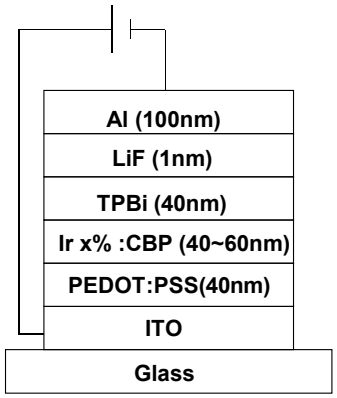

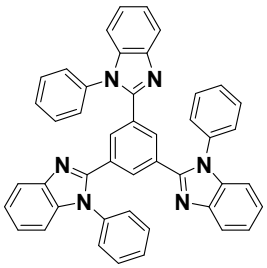

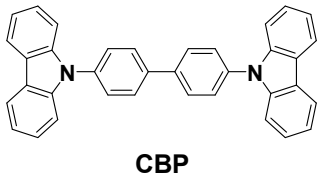

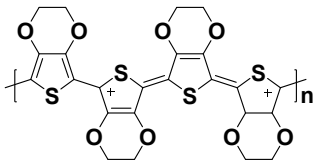

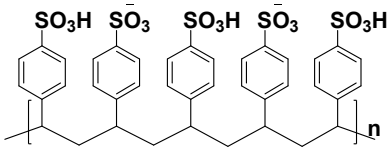

Dopant	Devices and doping levels
Ir-PON	**A1** (6 wt.-%), **A2** (8 wt.-%), **A3** (10 wt.-%)
Ir-POO	**B1** (6 wt.-%), **B2** (8 wt.-%), **B3** (10 wt.-%)
Ir-POB	**C1** (6 wt.-%), **C2** (8 wt.-%), **C3** (10 wt.-%)

Figure 6. General configuration of the PHOLED devices and the molecular structures of the relevant functional materials used in these devices.

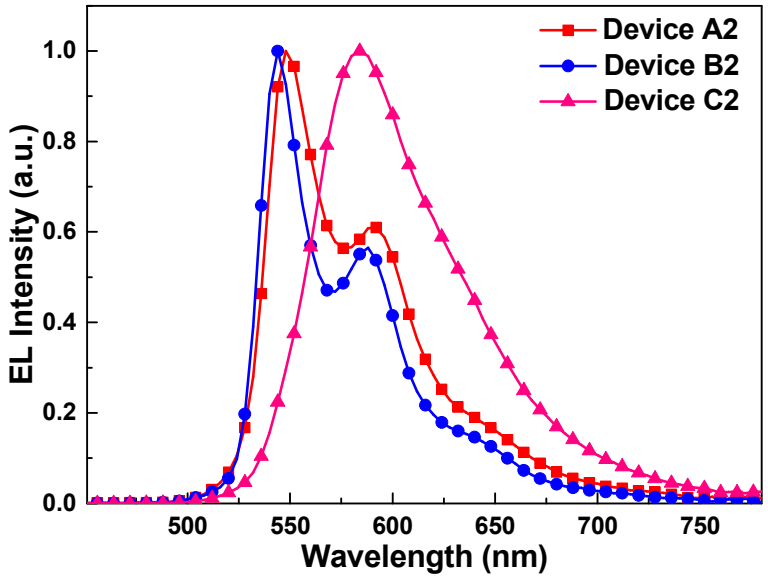

Figure 7. The EL spectra of device **A2**, **B2** and **C2** at *ca.* 10V.

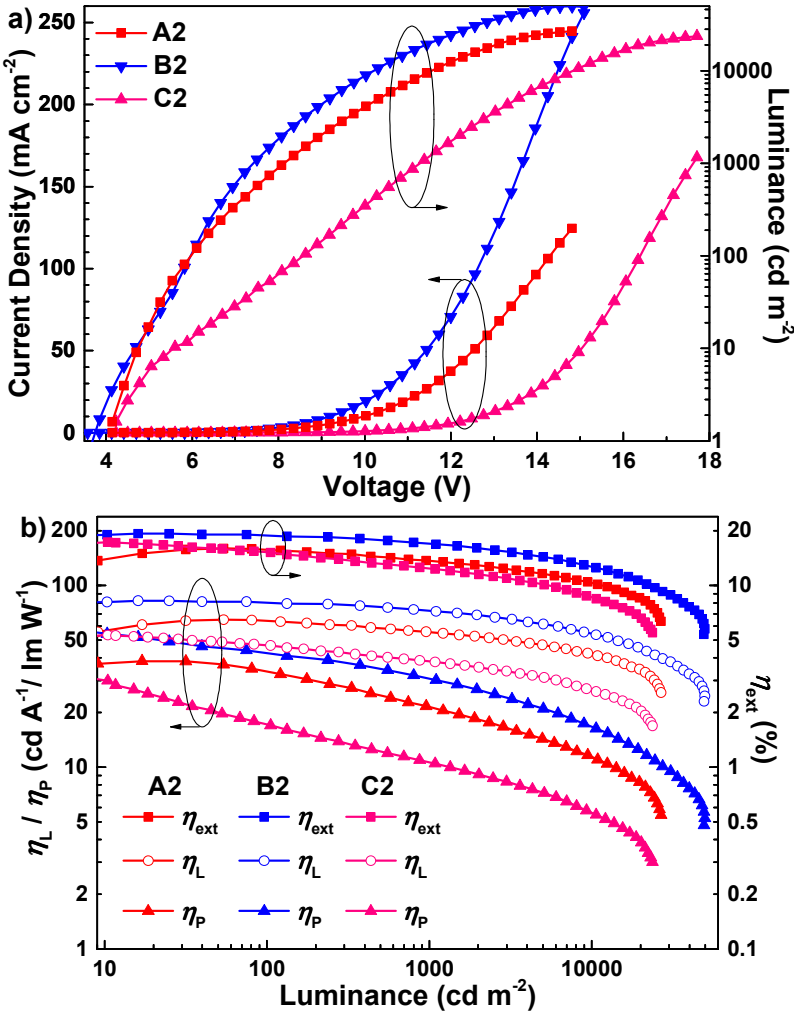

Figure 8. a) The Current Density-Voltage-Luminance(*J-V-L*) curves and b) the efficiency *versus* luminance of device **A2**, **B2** and **C2**.

Under a proper forward bias, all devices can emit intense electroluminescence (EL). The turn-on voltages (at a luminance of 1 cd m^{-2}) of these devices are relatively low, ranging from 3.6 V to 4.5 V, which is beneficial for obtaining high power efficiency. The EL spectra (**Figure 7**) of these devices are virtually identical to the PL spectra of the corresponding dopants, indicating the same origins of EL emissions as those of their PL emissions. No emission from CBP has been detected for these devices even at the doping level of 6 wt.-%, indicating the complete and efficient energy transfer from the host excitons to phosphorescent dopants. The current

density-voltage-luminance (*J-V-L*) relationships and EL efficiencies-luminance curves are showed in **Figure 8** and **Figure S4**. Detailed EL results are listed in **Table 5**. The device **B2** based on **Ir-POO** at a doping level of 8 wt.-% eventually exhibit the highest EL efficiency among all the devices. A maximum external quantum efficiency (η_{ext}) of 19.3%, a maximum current efficiency (η_L) of 82.5 cd A^{-1} and a maximum power efficiency (η_P) of 57.3 lm W^{-1} have been achieved. In fact, device **B3** with 10 wt.-% doping level of **Ir-POO** can even compare with device **B2** in view of its decent EL efficiencies with η_{ext} of 18.1%, η_L of 76.8 cd A^{-1} and η_P of 53.7 lm W^{-1}. Even at the doping level of 6 wt.-%, device **B1** can still maintain η_{ext} of 15.7%, η_L of 67.4 cd A^{-1} and η_P of 40.9 lm W^{-1}, which even outperforms our previously vacuum-deposited devices based on the phosphorescent analog of **Ir-POO** bearing cyclometalating ligand containing phenylsulfone (SO_2Ph) moiety.[17-18] Moreover, these phenomenal EL performances will definitely put the concerned devices among the most efficient solution-processed yellow-emitting OLEDs.[48] As for devices based on **Ir-PON**, their overall efficiencies were lower than those based on **Ir-POO**. The relatively lower Φ_p of **Ir-PON** both in solution (*ca.* 0.39) and in film (*ca.* 0.42) than those of **Ir-POO** (*ca.* 0.62 and 0.56, respectively) should be one of the reasons. However, a maximum η_{ext} of 16.0%, η_L of 64.9 cd A^{-1} and η_P of 38.4 lm W^{-1} are still achieved by device **A2** with 8 wt.-% doping level of **Ir-PON**. Devices based on **Ir-POB** also show relatively lower efficiencies compared with those with **Ir-POO** as emitter. Device **C2** doped with 8 wt.-% doping level of **Ir-POB** delivers the best EL performances with a maximum η_{ext} of 17.3%, η_L of 53.4 cd A^{-1} and η_P of 31.6 lm W^{-1}. Even though devices doped with **Ir-PON** and **Ir-POB** show inferior EL performances compared with those based on **Ir-POO**, they still outperform the vacuum-deposited devices doped with their analogs bearing SO_2Ph moiety.[17-18] No doubt, the suitable HOMO and LUMO levels of these asymmetric *tris*-heteroleptic Ir(III)

complexes with respect to those of CBP and TPBi certainly contribute to the exceptional EL performances of these devices. However, the inherent features of charge carrier injection associated with these asymmetric *tris*-heteroleptic Ir(III) complexes should mainly account for the advanced EL performances by their enhanced trapping ability for both kinds of charge carriers to improve the efficiency of charge recombination. From the results in **Figure 5b**, the contribution from the charge carrier transporting ability of these asymmetric *tris*-heteroleptic Ir(III) complexes to their impressive EL results should be in a subordinate position. Due to the triplet-triplet annihilation (TTA), all devices showed gradual efficiency roll-off with the increase of luminance/current density (**Table 5**).[49] Nevertheless, the EL efficiencies as high as 16.9%, 71.8 cd A^{-1} and 30.9 lm W^{-1} can still be maintained by device **B2** at even at a luminance of 1000 cd m^{-2}. Both these EL and the single carrier devices results validate the effectiveness of PhFlPO moiety for facilitating excellent EI/ET, indicating the great potential of PhFlPO moiety in constructing functionalized phosphorescent emitters with excellent EI/ET properties. Considering the quite simple structures of these OLEDs, there is still a large scope for further enhancement of the EL performance of these devices.

Table 5. EL performance of OLEDs based on the asymmetric *tris*-heteroleptic Ir^{III} complexes

Device	$V_{turn\text{-}on}$ (V)	Luminance L_{max} (cd m^{-2})[a]	η_{ext} (%)	η_L (cd A^{-1})	η_P (lm W^{-1})	λ_{max} (nm)[d]
A1	4.5	23499 (14.6)	9.9 (6.2)[a]	41.8 (6.2)	21.9 (5.9)	548
			9.8[b]	41.2	21.0	(0.441, 0.552)
			8.7[c]	36.7	13.9	
A2	4.1	26744 (14.8)	16.0 (5.5)	64.9 (5.5)	38.4 (5.0)	548
			15.7	63.6	33.6	(0.458. 0.536)
			13.7	55.7	21.5	
A3	4.2	20413 (14.5)	9.8 (5.6)	40.9 (5.6)	23.8 (5.0)	548
			9.3	38.9	19.6	(0.447, 0.546)
			8.0	33.9	12.7	

B1	3.9	37189 (13.9)	15.7 (5.5)	67.4 (5.5)	40.9(4.8)	544
			15.4	66.6	35.8	(0.426, 0.566)
			13.3	57.0	24.6	
B2	3.6	49648 (14.8)	19.3 (5.0)	82.5 (5.0)	57.3 (4.4)	544
			18.8	80.9	42.4	(0.439, 0.554)
			16.9	71.8	30.9	
B3	3.9	40944 (14.0)	18.1 (4.8)	76.8 (4.8)	53.7 (4.5)	544
			17.5	74.1	43.9	(0.440, 0.552)
			15.9	67.7	32.4	
C1	4.4	19722 (14.6)	13.6 (6.1)	42.4 (6.1)	22.1 (5.8)	580
			13.3	41.7	18.5	(0.538, 0.459)
			11.4	35.3	12.9	
C2	4.2	23683 (17.1)	17.3 (5.6)	53.4 (5.6)	31.6 (5.0)	584
			15.2	46.7	17.3	(0.546, 0.452)
			12.4	38.2	10.6	
C3	4.5	9118 (15.7)	15.3 (6.2)	46.2 (6.2)	23.5 (6.2)	584
			14.6	44.5	23.3	(0.546, 0.452)
			12.9	38.9	13.6	

[a] Maximum values of the devices. Values in parentheses are the voltages at which they were obtained. [b] Values collected at 100 cd m^{-2}. [c] Values collected at 1000 cd m^{-2}. [d] Values were collected at *ca.* 10 V, and CIE coordinates (x, y) are shown in parentheses.

CONCLUSION

Three asymmetric *tris*-heteroleptic Ir^{III} complexes containing PhFlPO moiety have been successfully developed. The strong EI/ET ability associated with the PhFlPO moiety can effectively optimize charge carrier injection/transporting behaviors of the asymmetric *tris*-heteroleptic Ir^{III} complexes through combination with HI/HT groups. Thus, the solution-processed OLEDs doped with these asymmetric complexes can achieve outstanding EL performances with a maximum η_{ext} of 19.3%, η_L of 82.5 cd A^{-1} and η_P of 57.3 lm W^{-1}. These excellent efficiencies are even higher than our previously reported vacuum-deposited OLEDs and place the concerned devices among the most efficient solution-processed yellow-emitting OLEDs. These results demonstrate that the PhFlPO moiety can be an excellent alternative to the widely used $POPh_2$/$POPh_3$ moieties to endow phosphorescent emitters and other functional

materials with superior EI/ET properties.

ASSOCIATED CONTENT

Supporting Information

Single crystal data for **Ir-PON**. Low temperature PL spectra and some EL data. This information is available free of charge via the Internet at http://pubs.acs.org.

AUTHOR INFORMATION

Corresponding Author

*Fax: +86-029-82663914 (G.Z.). E-mail: zhougj@mail.xjtu.edu.cn (G.Z.); zhaoxinwu@mail.xjtu.edu.cn (Z.W.).

Notes

The authors declare no competing financial interest.

ACKNOWLEDGEMENTS

This research was financially supported by the National Natural Science Foundation of China (no. 21572176, 20902072), the Fundamental Research Funds for the Central Universities (cxtd2015003), the China Postdoctoral Science Foundation (Grant no. 20130201110034, 2014M562403), the Program for New Century Excellent Talents in University, the Ministry of Education of China (NECT-09-0651), the Key Creative Scientific Research Team in Yulin City of Shaanxi Province. The financial supporting from State Key Laboratory for Mechanical Behavior of Materials is also acknowledged.

REFERENCES

(1) Baldo, M. A.; O'Brien, D. F.; You, Y.; Shoustikov, A.; Sibley, S.; Thompson, M. E.; Forrest, S. R., Highly efficient phosphorescent emission from organic electroluminescent devices. *Nature* **1998,** *395*, 151-154.

(2) Yuguang Ma; Houyu Zhang; Jiacong Shen; Che, C., Electroluminescence from triplet metal—ligand charge-transfer excited state of transition metal. *Synth. Met.* **1998,** *94*, 245-248.

(3) Xiao, L.; Chen, Z.; Qu, B.; Luo, J.; Kong, S.; Gong, Q.; Kido, J., Recent progresses on materials for electrophosphorescent organic light-emitting devices. *Adv. Mater.* **2011,** *23*, 926-952.

(4) Tao, Y.; Yang, C.; Qin, J., Organic host materials for phosphorescent organic light-emitting diodes. *Chem. Soc. Rev.* **2011,** *40*, 2943-2970.

(5) Ying, L.; Ho, C. L.; Wu, H.; Cao, Y.; Wong, W. Y., White polymer light-emitting devices for solid-state lighting: materials, devices, and recent progress. *Adv. Mater.* **2014,** *26*, 2459-2473.

(6) Reineke, S.; Lindner, F.; Schwartz, G.; Seidler, N.; Walzer, K.; Lussem, B.; Leo, K., White organic light-emitting diodes with fluorescent tube efficiency. *Nature* **2009,** *459*, 234-238.

(7) Zhou, G.; Wong, W.-Y.; Yang, X., New Design Tactics in OLEDs Using Functionalized 2-Phenylpyridine-Type Cyclometalates of Iridium(III) and Platinum(II). *Chem. Asian J.* **2011,** *6*, 1706-1727.

(8) Wong, W.-Y.; Ho, C.-L., Functional metallophosphors for effective charge carrier injection/transport: new robust OLED materials with emerging applications. *J. Mater. Chem.* **2009,** *19*, 4457-4482.

(9) Chaskar, A.; Chen, H. F.; Wong, K. T., Bipolar host materials: a chemical approach for highly efficient electrophosphorescent devices. *Adv. Mater.* **2011,** *23*, 3876-3895.

(10) Duan, L.; Qiao, J.; Sun, Y.; Qiu, Y., Strategies to design bipolar small molecules for OLEDs: donor-acceptor structure and non-donor-acceptor structure. *Adv. Mater.* **2011,** *23*, 1137-1144.

(11) Shirota, Y.; Kageyama, H., Charge Carrier Transporting Molecular Materials and Their Applications in Devices. *Chem. Rev.* **2007,** *107*, 953-1010.

(12) Shih, C.-H.; Rajamalli, P.; Wu, C.-A.; Chiu, M.-J.; Chu, L.-K.; Cheng, C.-H., A high triplet energy, high thermal stability oxadiazole derivative as the electron transporter for highly efficient red, green and blue phosphorescent OLEDs. *J. Mater. Chem. C* **2015,** *3*, 1491-1496.

(13) Oyston, S.; Wang, C.; Hughes, G.; Batsanov, A. S.; Perepichka, I. F.; Bryce, M. R.; Ahn, J. H.; Pearson, C.; Petty, M. C., New 2,5-diaryl-1,3,4-oxadiazole–fluorene hybrids as electron transporting materials for blended-layer organic light emitting diodes. *J. Mater. Chem.* **2005,** *15*, 194-203.

(14) Xu, Z.; Li, Y.; Ma, X.; Gao, X.; Tian, H., Synthesis and properties of iridium complexes based 1,3,4-oxadiazoles derivatives. *Tetrahedron* **2008,** *64*, 1860-1867.

(15) Zhao, J.; Yu, Y.; Yang, X.; Yan, X.; Zhang, H.; Xu, X.; Zhou, G.; Wu, Z.; Ren, Y.; Wong, W. Y., Phosphorescent Iridium(III) Complexes Bearing Fluorinated Aromatic Sulfonyl Group with Nearly Unity Phosphorescent Quantum Yields and Outstanding Electroluminescent Properties. *ACS Appl. Mater. Interfaces* **2015,** *7*, 24703-24714.

(16) Zhou, G.; Ho, C.-L.; Wong, W.-Y.; Wang, Q.; Ma, D.; Wang, L.; Lin, Z.; Marder, T. B.; Beeby, A., Manipulating Charge-Transfer Character with Electron-Withdrawing Main-Group Moieties for the Color Tuning of Iridium Electrophosphors. *Adv. Funct. Mater.* **2008,** *18*, 499-511.

(17) Xu, X.; Yang, X.; Wu, Y.; Zhou, G.; Wu, C.; Wong, W. Y., tris-Heteroleptic Cyclometalated Iridium(III) Complexes with Ambipolar or Electron Injection/Transport Features for Highly Efficient Electrophosphorescent Devices. *Chem. Asian J.* **2015,** *10*, 252-262.

(18) Xu, X.; Yang, X.; Dang, J.; Zhou, G.; Wu, Y.; Li, H.; Wong, W.-Y., Trifunctional IrIII ppy-type asymmetric phosphorescent emitters with ambipolar features for highly efficient electroluminescent devices. *Chem. Commun.* **2014,** *50*, 2473-2476.

(19) Zhou, G.; Wang, Q.; Ho, C.-L.; Wong, W.-Y.; Ma, D.; Wang, L.; Lin, Z., Robust Tris-Cyclometalated Iridium(III) Phosphors with Ligands for Effective Charge Carrier Injection/Transport: Synthesis, Redox, Photophysical, and Electrophosphorescent Behavior. *Chem. Asian J.* **2008,** *3*, 1830-1841.

(20) Zhou, G.; Yang, X.; Wong, W.-Y.; Wang, Q.; Suo, S.; Ma, D.; Feng, J.; Wang, L., A Robust Yellow-Emitting Metallophosphor with Electron-Injection/-Transporting Traits for Highly Efficient White Organic Light-Emitting Diodes. *Chemphyschem* **2011,** *12*, 2836-2843.

(21) Wang, B.; Lv, X.; Pan, B.; Tan, J.; Jin, J.; Wang, L., Benzimidazole–phosphine oxide hybrid electron transporters for unilateral homogeneous phosphorescent organic light-emitting diodes with enhanced power efficiency. *J. Mater. Chem. C* **2015,** *3*, 11192-11201.

(22) Ban, X.; Jiang, W.; Sun, K.; Xie, X.; Peng, L.; Dong, H.; Sun, Y.; Huang, B.; Duan, L.; Qiu, Y., Bipolar host with multielectron transport benzimidazole units for low operating voltage and high power efficiency solution-processed phosphorescent OLEDs. *ACS Appl. Mater. Interfaces* **2015,** *7*, 7303-7314.

(23) Hudson, Z. M.; Helander, M. G.; Lu, Z.-H.; Wang, S., Highly efficient orange electrophosphorescence from a trifunctional organoboron-Pt(ii) complex. *Chem. Commun.* **2011,** *47*, 755-757.

(24) Yang, X.; Sun, N.; Dang, J.; Huang, Z.; Yao, C.; Xu, X.; Ho, C.-L.; Zhou, G.; Ma, D.; Zhao, X.; Wong, W.-Y., Versatile phosphorescent color tuning of highly efficient borylated iridium(iii) cyclometalates by manipulating the electron-accepting capacity of the dimesitylboron group. *J. Mater. Chem. C* **2013,** *1*, 3317-3326.

(25) Jeon, S. O.; Lee, J. Y., Phosphine oxide derivatives for organic light emitting diodes. *J. Mater. Chem.* **2012,** *22*, 4233-4243.

(26) Deng, L.; Zhang, T.; Wang, R.; Li, J., Diphenylphosphorylpyridine-functionalized iridium complexes for high-efficiency monochromic and white organic light-emitting diodes. *J. Mater. Chem.* **2012,** *22*, 15910-15918.

(27) Fan, C.; Li, Y.; Yang, C.; Wu, H.; Qin, J.; Cao, Y., Phosphoryl/Sulfonyl-Substituted Iridium Complexes as Blue Phosphorescent Emitters for Single-Layer Blue and White Organic Light-Emitting Diodes by Solution Process. *Chem. Mater.* **2012,** *24*, 4581-4587.

(28) Zhu, M.; Li, Y.; Miao, J.; Jiang, B.; Yang, C.; Wu, H.; Qin, J.; Cao, Y., Multifunctional homoleptic iridium(III) dendrimers towards solution-processed nondoped electrophosphorescence with low efficiency roll-off. *Org. Electron.* **2014,** *15*, 1598-1606.

(29) Tian, W.; Qi, Q.; Song, B.; Yi, C.; Jiang, W.; Cui, X.; Shen, W.; Huang, B.; Sun, Y., A bipolar homoleptic iridium dendrimer composed of diphenylphosphoryl and diphenylamine dendrons for highly efficient non-doped single-layer green PhOLEDs. *J. Mater. Chem. C* **2015,** *3*, 981-984.

(30) Baumgartner, T., Insights on the design and electron-acceptor properties of conjugated organophosphorus materials. *Acc. Chem. Res.* **2014,** *47*, 1613-1622.

(31) Baumgartner, T.; Réau, R., Organophosphorus π-Conjugated Materials. *Chem. Rev.* **2006,** *106*, 4681-4727.

(32) Crassous, J.; Reau, R., pi-Conjugated phosphole derivatives: synthesis, optoelectronic functions and coordination chemistry. *Dalton Trans.* **2008,** 6865-6876.

(33) Hissler, M.; Lescop, C.; Réau, R., Organophosphorus π-conjugated materials: the rise of a new field. *J. Organomet. Chem.* **2005,** *690*, 2482-2487.

(34) Ren, Y.; Baumgartner, T., Combining form with function - the dawn of phosphole-based functional materials. *Dalton Trans.* **2012,** *41*, 7792-7800.

(35) Hobbs, M. G.; Baumgartner, T., Recent Developments in Phosphole-Containing Oligo- and Polythiophene Materials. *Eur. J. Inorg. Chem.* **2007,** *2007*, 3611-3628.

(36) Sheldrick, G. M. SHELXL-97: Program for Crystal Structure Refinement; University of Göttingen: Göttingen, Germany, 1997.

(37) Wadt, W. R.; Hay, P. J., Ab initio effective core potentials for molecular calculations. Potentials for main group elements Na to Bi. *J. Chem. Phys.* **1985,** *82*, 284-298.

(38) Hay, P. J.; Wadt, W. R., Ab initio effective core potentials for molecular calculations. Potentials for the transition metal atoms Sc to Hg. *J. Chem. Phys.* **1985,** *82*, 270-283.

(39) Frisch, M. J.; Trucks, G. W.; Schlegel, H. B.; Scuseria, G. E.; Robb, M. A.; Cheeseman, J. R.; Scalmani, G. B., V.; ; Mennucci, B.; Petersson, G. A.; Nakatsuji, H.; Caricato, M. L., X.; ; Hratchian, H. P.; Izmaylov, A. F.; Bloino, J.; Zheng, G.; Sonnenberg, J. L.; Hada, M.; Ehara, M.; Toyota, K.; Fukuda, R.; Hasegawa, J.; Ishida, M.; Nakajima, T.; Honda, Y.; Kitao, O.; Nakai, H.; Vreven, T.; Montgomery, J. A., Jr.;; Peralta, J. E.; Ogliaro, F.; Bearpark, M.; Heyd, J. J.; Brothers, E.; Kudin, K. N.; Staroverov, V. N.; Kobayashi, R.; Normand, J.; Raghavachari, K.; Rendell, A.; Burant, J. C.; Iyengar, S. S.; Tomasi, J.; Cossi, M.; Rega, N.; Millam, J. M.; Klene, M.; Knox, J. E.; Cross, J. B.; Bakken, V.; Adamo, C.; Jaramillo, J.; Gomperts, R.; Stratmann, R. E.; Yazyev, O.; Austin, A. J.; Cammi, R.; Pomelli, C.; Ochterski, J. W.; Martin, R. L.; Morokuma, K.; Zakrzewski, V. G.; Voth, G. A.; Salvador, P.; Dannenberg, J. J.; Dapprich, S.; Daniels, A. D.; Farkas, O.; Foresman, J. B.; Ortiz, J. V.; Cioslowski, J.; Fox, D. J., Gaussian 09, revision A.01; Gaussian, Inc.: Wallingford, CT, 2009.

(40) Kuninobu, Y.; Yoshida, T.; Takai, K., Palladium-catalyzed synthesis of dibenzophosphole oxides via intramolecular dehydrogenative cyclization. *J. Org. Chem.* **2011,** *76*, 7370-7376.

(41) Lamansky, S.; Djurovich, P.; Murphy, D.; Abdel-Razzaq, F.; Lee, H.-E.; Adachi, C.; Burrows, P. E.; Forrest, S. R.; Thompson, M. E., Highly Phosphorescent Bis-Cyclometalated Iridium Complexes: Synthesis, Photophysical Characterization, and Use in Organic Light Emitting Diodes. *J. Am. Chem. Soc.* **2001,** *123*, 4304-4312.

(42) Zhang, Y.; Song, M.; Huang, L., A novel blue-emitting Ir(III) complex with short excited state lifetime: Synthesis, structure, photophysical property, and electrophosphorescence performance. *J. Lumin.* **2012,** *132*, 2242-2246.

(43) Li, W.; Pan, Y.; Xiao, R.; Peng, Q.; Zhang, S.; Ma, D.; Li, F.; Shen, F.; Wang, Y.; Yang, B.; Ma, Y., Employing ~100% Excitons in OLEDs by Utilizing a Fluorescent Molecule with Hybridized Local and Charge-Transfer Excited State. *Adv. Funct. Mater.* **2014,** *24*, 1609-1614.

(44) Tsuboyama, A.; Iwawaki, H.; Furugori, M.; Mukaide, T.; Kamatani, J.; Igawa, S.; Moriyama, T.; Miura, S.; Takiguchi, T.; Okada, S.; Hoshino, M.; Ueno, K., Homoleptic Cyclometalated Iridium Complexes with Highly Efficient Red Phosphorescence and Application to Organic Light-Emitting Diode. *J. Am. Chem. Soc.* **2003,** *125*, 12971-12979.

(45) Chou, P. T.; Chi, Y., Phosphorescent dyes for organic light-emitting diodes. *Chem. Eur. J.* **2007,** *13*, 380-395.

(46) Caspar, J. V.; Sullivan, B. P.; Kober, E. M.; Meyer, T. J., Application of the energy gap law to the decay of charge transfer excited states, solvent effects. *Chem. Phys. Lett.* **1982,** *91*, 91-95.

(47) Zhang, S.; Chen, R.; Yin, J.; Liu, F.; Jiang, H.; Shi, N.; An, Z.; Ma, C.; Liu, B.; Huang, W., Tuning the Optoelectronic Properties of 4,4′-N,N′-Dicarbazole-biphenyl through Heteroatom Linkage: New Host Materials for Phosphorescent Organic Light-Emitting Diodes. *Org. Lett.* **2010,** *12*, 3438-3441.

(48) Fan, C.; Yang, C., Yellow/orange emissive heavy-metal complexes as phosphors in monochromatic and white organic light-emitting devices. *Chem. Soc. Rev.* **2014,** *43*, 6439-6469.

(49) Murawski, C.; Leo, K.; Gather, M. C., Efficiency roll-off in organic light-emitting diodes. *Adv. Mater.* **2013,** *25*, 6801-6827.

Table of Content

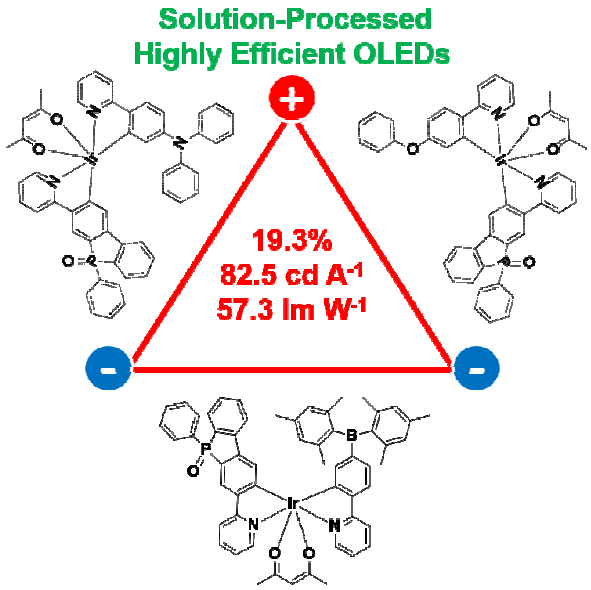
Solution-Processed
Highly Efficient OLEDs
19.3%
82.5 cd A-1
57.3 lm W-1
+
-
-
P
O
B
Ir
N
N
O
O